EUROPEAN COMMISSION
JOINT RESEARCH CENTRE
Environment Institute
Renewable Energies
21020 - Ispra (VA) Italy

The Surface-Limited Transport Parameters of Hydrogen in the Reduced Activation Martensitic Steel Optifer-IVb

G.A. Esteban, A. Perujo, L.A. Sedano, K. Douglas,
B. Mancinelli, P.L. Ceroni, G.B. Cueroni

2000 **EUR 19624 EN**

The mission of EI is to carry out research in support of EU policy for the protection of the environment and the citizen.

Prime objectives of EI are to investigate the level and fate of contaminants in the air, water and soil, to assess the effects of those contaminants upon the environment and individuals and to promote a sustainable energy supply.

EUROPEAN COMMISSION
JOINT RESEARCH CENTRE
Environment Institute
Renewable Energies
21020 - Ispra (VA) Italy

The Surface-Limited Transport Parameters of Hydrogen in the Reduced Activation Martensitic Steel Optifer-IVb

G.A. Esteban, A. Perujo, L.A. Sedano, K. Douglas,
B. Mancinelli, P.L. Ceroni, G.B. Cueroni

2000 **EUR 19624 EN**

EUR 19624 EN

Printed in Italy

THE SURFACE-LIMITED TRANSPORT PARAMETERS OF HYDROGEN IN THE REDUCED ACTIVATION MARTENSITIC STEEL OPTIFER-IVb

G. A. Esteban, A. Perujo, L. A. Sedano, K. Douglas, B. Mancinelli, P. L. Ceroni, G. B. Cueroni

Commission of the European Communities
Joint Research Centre – Ispra Site
Environment Institute, Renewable Energy Unit
21020 Ispra (VA), Italy

ABSTRACT

Two gas evolution techniques (Permeation and Isovolumetric Desorption) have been used to obtain the hydrogen isotopes surface rate constants, adsorption σK_1 (mol $m^{-2}s^{-1}Pa^{-1}$) and recombination σK_2 ($mol^{-1}m^4s^{-1}$), in the martensitic steel OPTIFER-IVb. The permeation measurements were carried out in the temperature range 523 to 723 K with a deuterium driving pressure ranging from $5\cdot10^2$ to 10^5 Pa, whereas the isovolumetric desorption measurements were carried out in the temperature range 553 to 903 K with a protium driving pressure ranging from $4\cdot10^4$ to 10^5 Pa.

The deuterium surface rate constants obtained are:

$$\sigma K_1(\text{mol } m^{-2}s^{-1}Pa^{-1})=2.998\cdot10^{-8}\exp(-29230/(RT))$$

$$\sigma K_2(mol^{-1}m^4s^{-1})=2.838\cdot10^{-7}\exp(-28679/(RT))$$

The deuterium permeability obtained from the permeation measurements is:

$$\Phi(\text{mol } m^{-1}Pa^{-1/2}s^{-1})= 5.311\cdot10^{-8}\exp(-44988/(RT))$$

In very good agreement with the deuterium diffusive transport parameters previously measured using the isovolumetric desorption experiment.

The growth of oxide on the specimens has been evidenced and the quantitative impact on surface rate constant values reported.

SUMMARY

1. Introduction 1

2. Theory 2

3. Material 7

4. Permeation experiment 10
   4.1. The permeation facility 10
   4.2. The permeation experimental procedure 12
   4.3. Permeation modelling 14
      4.3.1. Intermediate permeation regime 14
      4.3.2. Hydrogen transport parameters evaluation 18
   4.4. Results for permeation experiment 20
      4.4.1. Permeation regime definition 20
      4.4.2. Results from permeation modelling 22

5. Isovolumetric desorption experiment 28
   5.1. The isovolumetric desorption facility 28
   5.2. The isovolumetric desorption experimental procedure 29
   5.3. Isovolumetric desorption modelling 31
      5.3.1. Surface-limited transport regime 31
      5.3.2. Surface rate constants evaluation 33
   5.4. Results for isovolumetric desorption experiment 34
      5.4.1. Transport regime 34
      5.4.2. Results from isovolumetric desorption modelling 35

6. Comparison of results 42

7. Conclusions 45

8. References 46

LIST OF TABLES

Table 1. Activation energy for the processes shown in Fig. 2. 4

Table 2. Chemical composition of OPTIFER-IVb and MANET-II (wt%). 8

Table 3. Derived permeation numbers (W)..... 27

LIST OF FIGURES

Figure 1. Potential energy distribution in a metal surface 3

Figure 2. Scheme of surface processes 4

Figure 3. Optical micrographs of OPTIFER-IVb..... 9

Figure 4. Schematic view of the permeation facility..... 11

Figure 5. Characteristic permeation curve. 13

Figure 6. Scheme of the permeation process through 1-d slab. 15

Figure 7. Graphic solution of the general equation for the steady-state permeation..... 19

Figure 8. Steady state permeation fluxes. Transport regime characterisation. 21

Figure 9. Fitting curves for permeation experimental results. 23

Figure 10. Arrhenius plot of the fitted adsorption constant (PT)..... 24

Figure 11. Arrhenius plot of the fitted recombination constant (PT). 25

Figure 12. Arrhenius plot of the fitted permeability (PT) 26

Figure 13. Schematic view of the isovolumetric desorption facility..... 28

Figure 14. Experimental result of IDT pressure increment and fitting 30

Figure 15. Normalised pressure release curves undertaken at the same temperature (745 K) at different pressures. 35

Figure 16. Arrhenius plot of the adsorption constant values 38

Figure 17. Arrhenius plot of the recombination constant values (IDT) 39

Figure 18. XPS spectrum of oxidised OPTIFER-IVb, showing the presence of Mn, Cr and Fe oxides. 40

Figure 19. Arrhenius plot of the Sieverts' constant values (IDT)..... 41

Figure 20. Arrhenius plot of adsorption rate constants 43

Figure 21. Arrhenius plot of recombination rate constants 44

1. INTRODUCTION

The suitability of ferritic-martensitic steels as blanket structural materials for thermonuclear fusion devices is well known. This class of steel has better swelling resistance, lower sensitivity to helium embrittlement and more suitable thermophysical properties than the austenitic stainless steels [1, 2].

A series of low activation martensitic steels (OPTIFER) has been developed as a potential material for the blanket structures of a future fusion device [3, 4]. Until recently the martensitic steel DIN 1.4914 (MANET) had been considered as the reference structural material for the design of a Demonstration reactor (DEMO). In comparison to MANET, the new group of OPTIFER steels exhibits better activation properties, since alloying elements, which produce long-lived activation products, have been substituted or eliminated. Thereby Mo and Nb were replaced by W and Ta, respectively, fulfilling the same metallurgical function whilst Ni was totally eliminated.

This group of CrWVTa steels are being investigated by metallurgical and mechanical examinations of non-irradiated specimens. OPTIFER-IVb has turned out to have quite an appropriate set of mechanical properties, showing a good balance between high fracture toughness, a low ductile-to-brittle transition temperature (DBTT) and a high creep strength.

Such a promising structural material needs a detailed analysis in relation with the H interaction characteristics. The hydrogen (H) diffusive transport parameters of OPTIFER-IVb, were assessed in previous works [5, 6]. The understanding of H transport parameters through the materials of fusion reactors at low H isotopes partial pressures (10^3 Pa and less) requires to consider another features describing the H transport other than those in the bulk of the material. Moreover, as partial pressures are lowered the surface processes, that affect the solution and release of the gas, increasingly influence the kynetics and ultimately determine the rates of transport; specially if oxide or other impurities are present on the material surface.

The present work is aimed to obtaining the H isotopes surface rate constants of adsorption σK_1 (mol $m^{-2}s^{-1}Pa^{-1}$) and recombination σK_2 ($mol^{-1}m^4s^{-1}$) in OPTIFER-IVb. These surface rate constants, together with the diffusive transport [5, 6], provide the necessary information to evaluate, by means of known numerical codes [7-10], the H Inventory in, Permeation through and Recycling from (IPR) the reactor walls and blanket structures. The values of such parameters are needed when analysing:

1. The IPR effects on the state of plasma and the process of tritium breeding.
2. The quantification of radiological hazards coming from tritium leakage and the assessment of tritium inventory.

The experimental methods used in deriving the H isotopes surface rate constants are: the Permeation Technique (PT), carried out over a temperature range of 523 to 723 K with a deuterium (H_D) driving pressure ranging from $5 \cdot 10^2$ to 10^5 Pa, and the Isovolumetric Desorption Technique (IDT), used over a temperature range of 553 to 903 K with a protium (H_P) driving pressure ranging from $4 \cdot 10^4$ to 10^5 Pa.

2. THEORY

In this section theory concerning surface effects in H transport within a metal is reported.

In many occasions it has been experimentally proved and theoretically studied [11-15] that under certain conditions (i.e. low pressure level, presence of impurities, degradation, oxidation of the surface), the H transport regime becomes surface limited, i.e. H transport within the material is limited by the physico-chemical reactions (adsorption, dissociation, desorption, recombination) occurring at the surface of the material, rather than diffusion limited, where H transport is limited by the diffusion of H atoms through the host matrix of the bulk of the material. In Figure 1 a scheme of the potential energy levels acquired by an H atom on and in the vicinity of an endothermic alloy surface is presented.

The complete group of processes occurring on the surface of the material is depicted in Figure 2. Where p is the H_2 gas partial pressure, c the H concentration at the

subsurface and θ the surface coverage, i.e. the occupation rate by H atoms of the available adsorption sites on the surface. The referred phenomenological constants k_i, i=1,…,8, are only functions of temperature; their activating energies, showed in Table 1, have been evaluated taking into account the potential energy barriers and wells depicted in Figure 1.

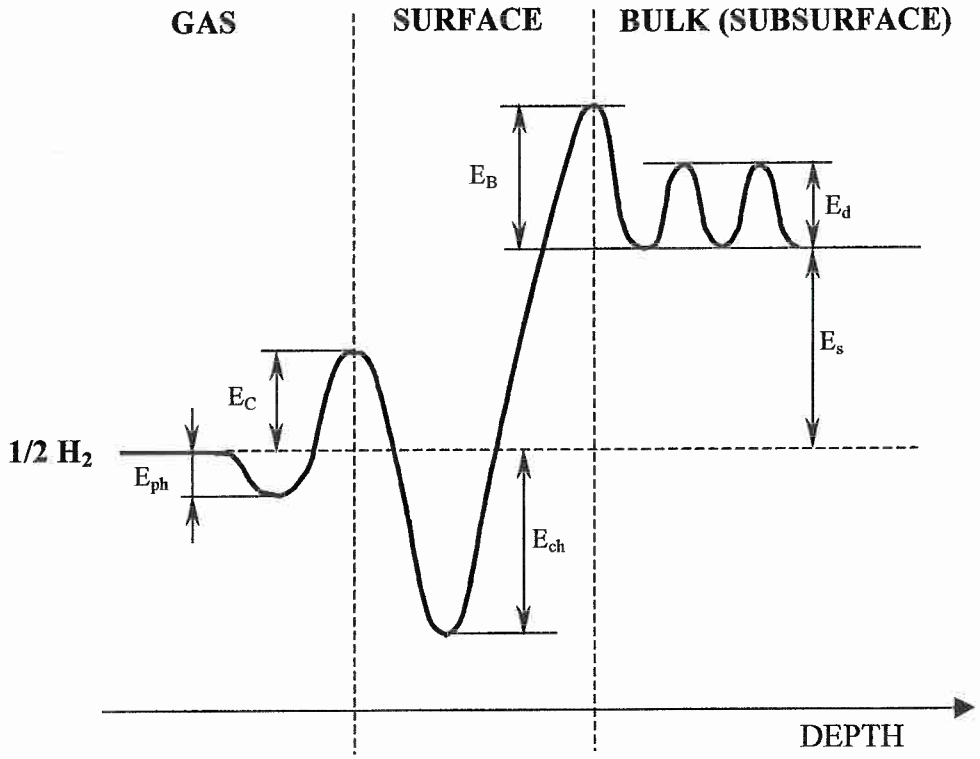

E_{ph}: physisorption energy. It is the binding energy the atoms of the physisorbed H_2 molecule are bound with to the surface metal due to Van der Waals' forces.

E_C: sticking energy. It is the energy barrier defining the sticking process; its value depends on the presence of impurities on the surface of the metal.

E_{ch}: chemisorption energy. It is the binding energy the adsorbed H atoms are bound to the surface metal due to atomic interaction.

E_B: desorption energy. It is the energy barrier a dissolved atom has to surmount in order to accede to an adsorption surface position from where recombination is able to proceed.

E_d: diffusion energy. It is the barrier a diffusing atom has to surmount in order to pass, within the lattice, from one solution site to another.

E_s: solution energy. It is the energy difference between a free atom and a dissolved one; depending on the sign of this energy the material is characterised as endothermic, $E_s>0$, or exothermic, $E_s<0$.

Figure 1. Potential energy distribution in a metal surface.

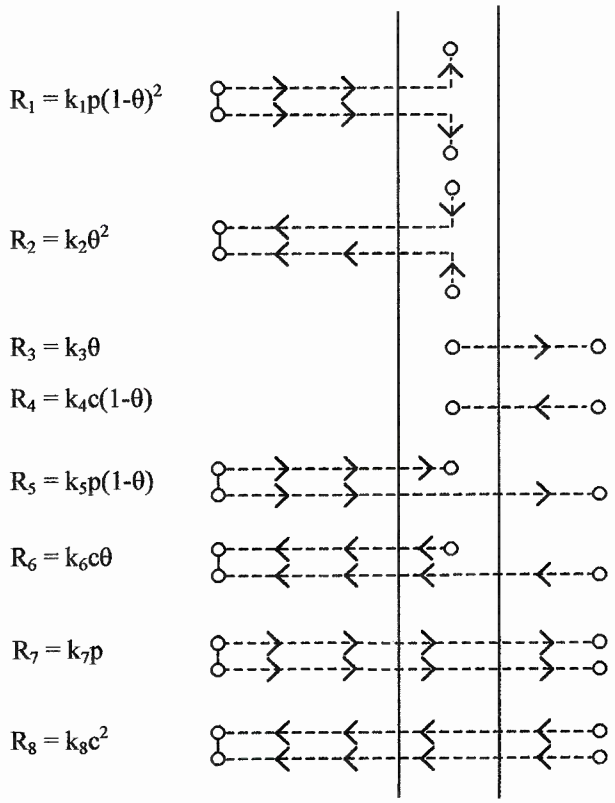

Figure 2. Scheme of surface processes.

Table 1. Activation energy for processes shown in Fig. 2. Values are for endothermic metal with $E_C<E_s+E_B$.

Phenomenological constant	k_1	k_2	k_3	k_4	k_5	k_6	k_7	k_8
Energy barrier	$2(E_C)$	$2(E_{ch}+E_C)$	$E_{ch}+E_s+E_B$	E_B	$E_C+E_s+E_B$	$E_{ch}+E_C+E_B$	$2(E_s+E_B)$	$2E_B$

A simple path followed by H atoms in the absorption may be the following:

The hydrogen atoms in molecular state may be physisorbed when interacting with the surface by means of Van der Waals forces and drop in the potential well E_{ph}. Then, owing to its temperature vibrational state, the molecules may surmount the sticking barrier E_C (this energy might be null provided a perfect cleaned surface state is assured) and pass to a chemisorption position where the H atoms remain "sticked" to

alloy atoms by strong bounds of electronic orbital sharing nature (R_1). Moreover, the binding between the two H atoms of each molecule are weak and dissociative adsorption occurs; from then on, hydrogen atoms behave individually when interacting with host lattice atoms. The next step, is the jump from the surface into the lattice bulk, where a total energy barrier $E_{ch}+E_s+E_B$ must be surmounted (R_3).

In a similar manner, the release path may be described as follows:

A dissolved H atom occupying a solution site in the part of the bulk close to the surface, i.e. subsurface, may surmount the desorption energy E_B and reach a surface chemisorption position (R_4). Then it may interact with other chemisorbed H atom resulting in the recombination of both atoms to form a free (or physisorbed) molecule; in this process an energy barrier of $E_{ch}+E_C$ must be surmounted (R_2).

Every H atom might not follow all the processes described above, since a H atom is capable of directly jumping from its molecular state to a subsurface solution site and conversely. This situation may be possible providing the surface coverage θ is high, $\theta\approx1$, so that in some cases adsorption site vacancies do not exist and H atoms are compelled to follow processes R_5 and R_6 or R_7 and R_8 (Fig. 2).

Assuming that equilibrium between surface and subsurface actually occurs [16], the surface coverage θ is proportional to the subsurface H concentration c and the H flux rates R_3 and R_4 cancel each other, so that the rest of the process rates are proportional either to the external H partial pressure p or to the square of the subsurface concentration c^2.

The evaluation of such process rates leads to consider one adsorption flux and one recombination flux. Hence, the H flux entering the material J, can be expressed as:

$$J=\sigma K_1 p-\sigma K_2 c^2 \qquad (1)$$

σK_1 (mol $m^{-2}s^{-1}Pa^{-1}$) and σK_2 ($m^4s^{-1}mol^{-1}$) being the adsorption and recombination rate constants, respectively. σ is the surface roughness expressing the quotient between the real and the geometrical areas of the surface.

If a specimen of material is exposed to a certain partial pressure of H, p, for enough time to reach a saturation state, an equilibrium concentration in the bulk, the same as the H subsurface concentration, c_{eq}, is reached. Thus recombinative and adsorptive fluxes show dynamic equilibrium cancelling each other:

$$0=\sigma K_1 p-\sigma K_2 c_{eq}^2 \qquad (2)$$

In the described equilibrium state Sieverts' law, $c_{eq}=K_s p^{1/2}$, is fulfilled. Hence, a direct relationship between surface rate constants, σK_1, σK_2, and Sieverts' constant, K_s, arises:

$$K_s = \sqrt{\frac{\sigma K_1}{\sigma K_2}} \qquad (3)$$

It is worth noting that once the Sieverts' constant is known and using the previous expression (3), it is only necessary to evaluate one of the surface rate constants in order to define completely the surface-limited H transport. Furthermore, the most reliable attempts in theoretically defining the surface-limited transport regime [13, 14] calculate the adsorption constant σK_1 rather than σK_2; for σK_1 can be easily evaluated in terms of a simple kinetic theory. The conclusions reached in those works propose the following expressions for the adsorption constant:

For Baskes' approximation [13]:

$$\sigma K_1 = \frac{2Cs\sigma}{(2mT)^{1/2}} \exp\left(\frac{-E_x}{RT}\right), \ (E_x=\max(0, E_s+E_d)) \qquad (4)$$

For Pick and Sonnenberg's approximation [14]:

$$\sigma K_1 = \frac{Cs\sigma}{(2mT)^{1/2}} \qquad (5)$$

C being a kinetic constant equal to 4.376 mol $K^{1/2}u^{1/2}Pa^{-1}m^{-2}s^{-1}$. "s" is the "sticking coefficient" expressing the probability that a H atom remains "sticked" to an adsorption surface site; it is activated with an energy of $2E_C$ because both the two atoms from the H_2 molecule must surpass the sticking barrier E_C:

$$s = s_0 \exp\left(\frac{-2E_C}{RT}\right) \qquad (6)$$

m is the H isotope atomic mass (a.m.u.), T the temperature (K) and R the ideal gas' constant (8.314 J $K^{-1}mol^{-1}$).

3. MATERIAL

The material studied is OPTIFER-IVb [3, 4]; a reduced-activation martensitic (RAM) 8% CrWVTa steel, heat number 986635, produced by Saarstahl GmbH (Germany).

The specimen for PT consisted of a thin disc with a 0.8-mm thickness and 22-mm diameter. This physical configuration of the specimen permits, on the one hand, to account for surface effects, if they are present, because large surface areas are available for transport in comparison with short diffusive lengths. On the other hand, it makes feasible the H isotopes transport study using an infinite-slab (1-d) geometry approximation.

The specimens for IDT consisted of four cylinders with a 6-mm diameter and 60-mm height. The specimen dimensions were defined in this manner to make feasible the H transport study using an infinite-cylinder (1-d radial) geometry approximation. Each batch tested consisted of four specimens to provide an appropriate signal-to-noise ratio in the experiments.

In both cases, PT and IDT, the specimens were machined from a rod of material supplied by Forschungszentrum Kalsruhe with the chemical composition (wt%) given in Table 2.

It can be noticed the elements producing long-lived activation products, those present in MANET (Table 2) such as Mb, Nb and Ni, are absent. The stabilising grain size alloying element Nb has been substituted by Ta, whereas Mo has been substituted by W and Ni has been completely eliminated.

Table 2. Chemical composition of OPTIFER IVb and MANET-II (wt%).

	OPTIFER-IVb	MANET-II
C	0.12	0.11
Cr	8.3	10.3
Nb	—	0.14
Ta	0.06	—
Mo	—	0.58
W	1.4	—
Ni	—	0.65
Mn	0.34	0.85
V	0.22	0.19
N	0.03	0.03
Fe	Balance	Balance

After machining, the specimens of steel underwent the normalising heat treatment that has demonstrated to confer the most appropriate set of mechanical properties [3]: austenizing at 1223 K for 0.5 h, fast cool, tempering at 1003 K for 3 h and finally slow cooling to room temperature. This heat treatment guarantees a fine pre-austenitic grain size, a fully martensitic phase and no pre-eutectoid carbide precipitation. In Figure 3 the microstructure of the steel can be observed; it shows the well-structured martensite consisting of fine laths.

The surface of the specimens was mechanically polished using a sequence of fine grain SiC abrasive paper and finally with 9, 6 and 3 μm diamond paste. Subsequently the specimens was degreased with acetone and ethanol, then rinsed in distilled water and finally dried in a vacuum furnace before insertion into the experimental rigs.

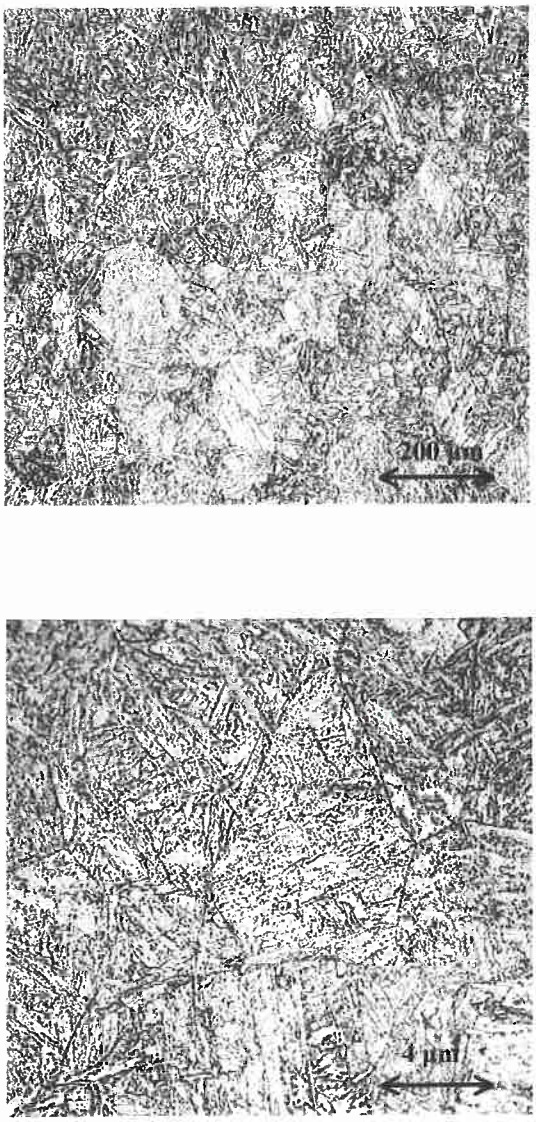

Figure 3. Optical micrographs of OPTIFER-IVb.

4. PERMEATION EXPERIMENT

4.1. The permeation facility

A schematic view of the permeation installation is shown in Figure 4. This installation and the procedure for a measurement has been described in earlier works [17-19]. Here we will briefly describe the experimental setup for completeness.

The rig comprises ultra high vacuum stainless steel components, such as the manually actuated leak valves, the calibrated volume (V1) and an extensive pipe-work.

The ultra high vacuum needed before any measurement is obtained by two pumping units (UHV1 and UHV2); both of them comprise a turbomolecular and a two-stage rotary pump. A good level of vacuum, about 10^{-6} Pa, is reached prior to system bakeout at 300 °C, and about 10^{-7} Pa, afterwards. Several Penning gauges (PG) together with a quadrupole mass spectrometer (QMS) control the quality of the vacuum reached.

The specimen (S) is placed between two flanges that are set into a resistance furnace allowing measurements at an experimental temperature of 773 K and lower. A nickel/chromium-nickel thermocouple (T1) held in a well drilled into one of the flanges permits the temperature control with stability of ± 1 K. Two gold O-rings ensures the specimen leak tightness and avoid any radial gas leak through the junctions between the specimen and the flanges.

The quadrupole mass spectrometer (QMS) monitories the gas purity, both the high pressure supplied from the cylinder and the permeated through the specimen. Thereby, it can be detected the presence of deleterious components that may induce a change of the specimen surface conditions, such as oxygen and water vapour from the air, or oil fumes from the pumping units.

A high-pressure transducer (HPT) and a pressure controller (PC) allow accurately testing the sample with the desired constant driving pressure level. A capacitance manometer (P1) measures the pressure increase due to permeation through the sample

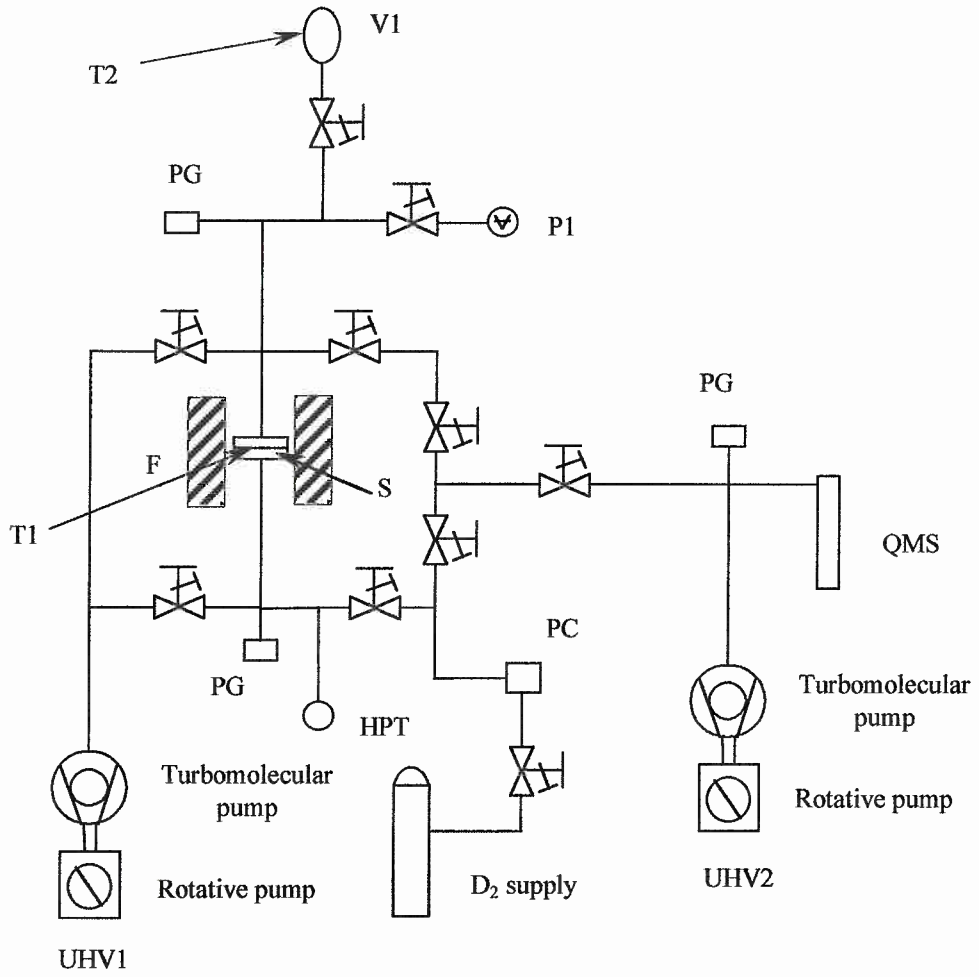

PG	Penning Gauge.	F	Furnace.
PC	Pressure controller.	HPT	High-pressure transducer.
QMS	Quadrupole mass spectrometer.	S	Specimen.
T1, T2	Nickel/chromium-nickel thermocouples.	P1	Capacitance manometer.
UHV	Ultra high vacuum pumping units.	V1	Calibrated volume.

Figure 4. Schematic view of the permeation facility.

into the low-pressure region. A calibrated volume (V1) permits, by gas expansion (Sieverts' method), to evaluate the effective volume of the low-pressure region and, thus, to transform the pressure increase in the quantity of permeated gas.

4.2. The permeation experimental procedure

The gas permeation technique intends to measure the H transport parameters (the surface-reaction rate constants if a surface-limited transport regime occurs, or the bulk transport parameters in case of a diffusive transport regime) by characterising the permeation of H through a thin slab of that material.

A single run of the experiment consists of holding one surface of the specimen at a certain high H pressure level, forcing the H permeation through the specimen to the low pressure region (Fig. 4). A capacitance manometer (P1) records the pressure increase in the low pressure volume; because this volume is known in every run, each pressure level may be evaluated as the total amount of permeated gas: Q(t). Likewise the pressure increase rate may be converted into the amount of gas permeated per sample unit area and time (gas flux, $J(t) = \frac{\partial Q(t)}{\partial t}$).

This single run is repeated for different driving pressures, provided by the pressure controller (PC), and temperatures, achieved with the resistance furnace (F).

From the instant when the high driving pressure forces permeation to the low-pressure region, the H permeation flux rises progressively with time until a steady-state permeation flux is reached. The modelling of the pressure increase (p(t)), due to the gas permeation in the low-pressure region, makes possible to derive the transport parameters in the diffusive or surface-limited transport regime. A characteristic permeation curve is depicted in Fig. 5.

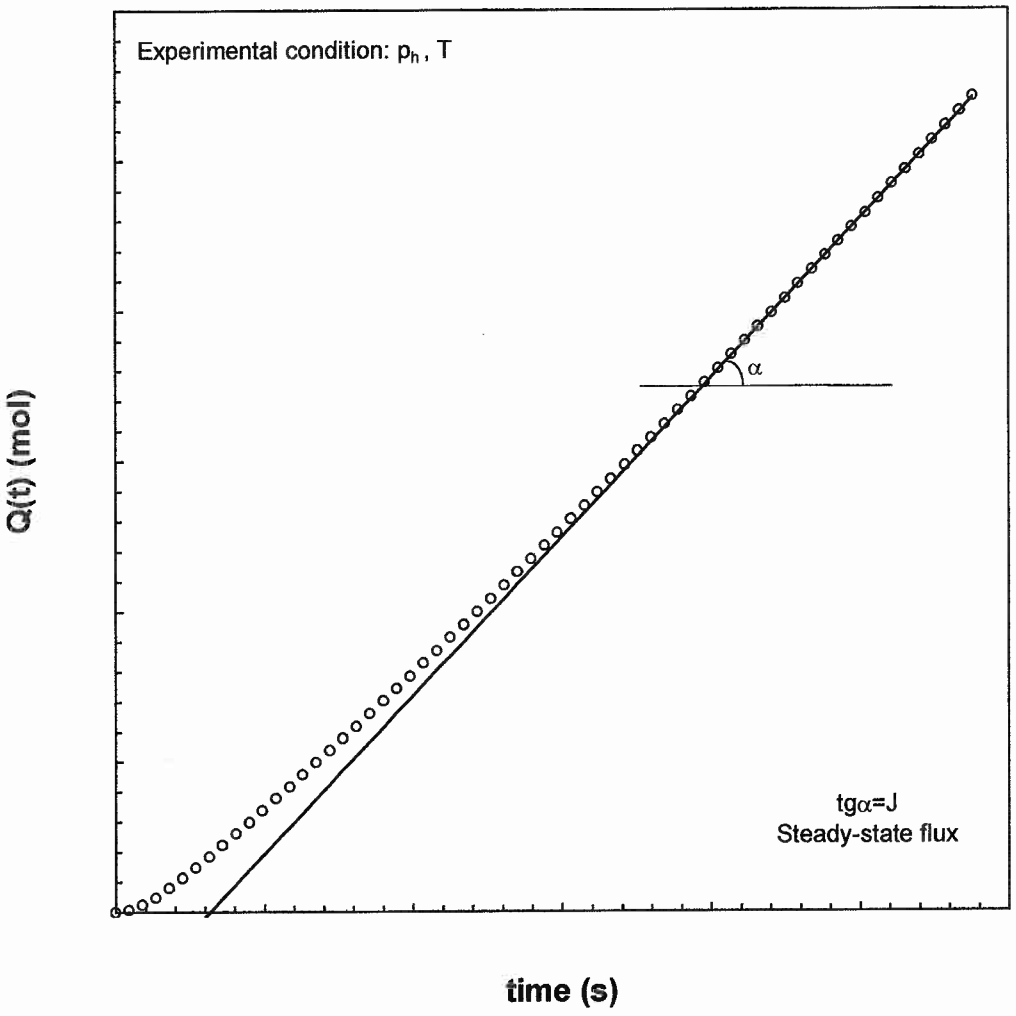

Figure 5. Characteristic permeation curve. ○ actual H permeated quantity; — expected H permeated quantity in the steady state.

The current PT experiment deals with an intermediate regime, neither purely diffusive nor surface-limited. An intermediate model provides direct evaluation of adsorption constant σK_1 and the permeability Φ by means of the study of the steady-state permeation at different levels of driving pressure and temperatures.

4.3. Permeation modelling

4.3.1. Intermediate permeation regime

The theoretical model applied analyses the intermediate transport regime; i.e. hydrogen transport kynetics is not exclusively limited either by diffusion within the bulk of the material or by transport at the surface, but a combination of both of them. Besides surface rate constants σK_1 and σK_2, this intermediate model allows assessing the permeability Φ (mol m^{-1} $Pa^{-1/2}s^{-1}$).

The intermediate transport model is currently applied for describing permeation runs when transport is not exclusively limited either by the diffusion through the bulk of the material or by the surface reactions [16-18]. Here we will briefly explain the model for completeness.

When a pure diffusive transport regime is verified the steady-state permeating H flux is proportional to the square root of the driving pressure as follows:

$$J = \frac{\Phi}{d} p_h^{1/2} \tag{7}$$

where the pressure level at the low pressure region has been neglected comparing to the high pressure level. d is the width of the specimen and p_h the driving pressure.

In case of a pure surface-limited transport regime, the steady-state permeating H flux is directly proportional to the driving pressure:

$$J = \frac{1}{2}\sigma K_1 p_h \tag{8}$$

In the majority of gas permeation experiences, as it is the present case, the steady-state H permeation flux maintains a proportional relation with an intermediate power of the

pressure ranging between 0.5 and 1. This fact means that, both, surface and diffusion effects affect the permeation. The model developed hereafter considers the combination of such effects.

The scheme of steady-state permeation through a infinite slab in a intermediate regime is depicted in Figure 6; wherein all the involved H fluxes are represented, either those coming from surface reaction processes, recombination $J_{o,h}=\sigma_h K_{2,h} c_h^2$, $J_{o,l}=\sigma_l K_{2,l} c_l^2$, and adsorption $J_{i,h}=\sigma_h K_{1,h} p_h$ $J_{i,l}=\sigma_l K_{1,l} p_h$, or the diffusive flux $J_d = -D\frac{\partial c(x)}{\partial x}$. The sub-indexes indicate "o" out, "i" in, "l" low-pressure-region, "h" high-pressure-region, "d" diffusive.

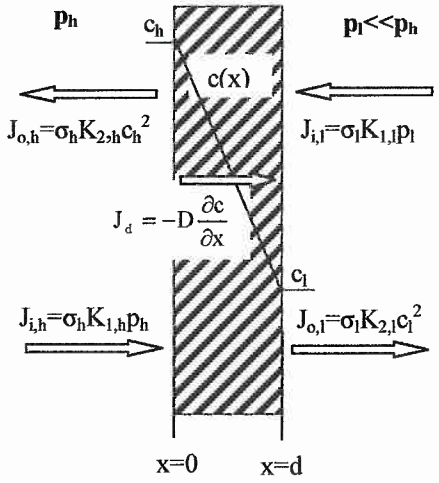

Figure 6. Scheme of the permeation process through 1-d slab.

It is worth noting that only the steady-state permeation is accounted at this stage. That is why a lineal profile of concentration is built up within the bulk of material; such profile remains invariable during the steady-state permeation so that no H inventory accumulation or diminution is produced. Moreover, all the fluxes referred above can be considered constant.

The following hypotheses are assumed:

-Symmetric slab: $\sigma_h K_{1,h}=\sigma_l K_{1,l}=\sigma K_1$, ,$\sigma_h K_{2,h}=\sigma_l K_{2,l}= \sigma K_2$.

-Low pressure side simplification: $p_h >> p_l \approx 0$, $J_{i,l} = \sigma K_1 p_l = 0$.

Some new parameters are defined to simplify the mathematical study:

-The "reduced concentration": $C(x)=\frac{c(x)}{c_{eq}}$; being $c_{eq}=K_s p_h^{1/2}$ the equilibrium H concentration reached when the entire specimen (i.e. both sides of it) is exposed to the pressure p_h.

-The "permeation number": $W=\frac{\sigma K_1 p_h}{\frac{\Phi}{d}\sqrt{p_h}}=\frac{\sigma K_1 d}{\Phi}\sqrt{p_h}$, is the quotient of the adsorption flux at x=0 (high-pressure side) and the steady-state flux in a pure diffusive regime. It states the gas transport regime class, i.e. whether the regime is pure diffusive, W>>1, or it is pure surface-limited, W<<1, or it is an intermediate transport regime between the two previous ones.

Considering the H mass balance at the surface facing the low pressure region, x=d (Fig. 6):

$$J_d=J_{o,I}-J_{i,I}\approx J_{o,I}=J \tag{9}$$

From this expression, taking into account the lineal profile of H concentration, the diffusive flux is easily evaluated:

$$D\frac{c_h-c_l}{d}=\sigma K_2 c_l^{\,2} \tag{10}$$

Bearing in mind the reduced concentration, C, and the permeation number, W, previously defined, and the relation between surface rate constants and Sieverts' constant (3), eq. (10) can be transformed into:

$$C_h-C_l=WC_l \tag{11}$$

Considering the H mass balance at the surface facing the high pressure region, x=0, and eq. (9):

$$J_{i,h}-J_{o,h}=J_d=J_{o,I} \tag{12}$$

Attending fluxes definition:

$$\sigma K_1 p_h-\sigma K_2 c_h^{\,2}=\sigma K_2 c_l^{\,2} \tag{13}$$

Once again, considering the defined parameters W, C_h and C_l, Sieverts' law and eq. (3), the previous equation (13) can be transformed into the more simplified expression:

$$C_h^{\,2}=1-C_l^{\,2} \tag{14}$$

From equations (11) and (14) the general equation for the steady-state permeation through a symmetric membrane can be derived:

$$W^2C_l^4+2WC_l^3+2C_l^2=1 \qquad (15)$$

The reduced concentration at the subsurface corresponding to the low pressure region x=d, can be expressed in terms of the H fluxes:

$$C_l^{\,2}=\frac{c_l^{\,2}}{c_{eq}^{\,2}}=\frac{\sigma K_2 c_l^{\,2}}{\sigma K_2 K_s^{\,2} p_h}=\frac{J}{\sigma K_1 p_h}=\frac{J}{J_{i,h}} \qquad (16)$$

The general equation (15) establishes a relation between this reduced concentration $C_l^{\,2}=\frac{J}{\sigma K_1 p_h}$ and the permeation number $W=\frac{\sigma K_1 d}{\Phi}\sqrt{p_h}$; i.e., the directly measurable quotient $\frac{J}{p_h}$ is function of p_h through the unknown parameters σK_1 and Φ.

From the expression (15) it can be noticed that for low permeation numbers W<<1, the steady-state permeation equation becomes:

$$2C_l^{\,2}=2\frac{J}{J_{i,h}}=1 \qquad (17)$$

$$J=\frac{1}{2}J_{i,h}=\frac{1}{2}\sigma K_1 p_h \qquad (18)$$

Which is the steady-state permeation equation for a pure surface-limited regime (eq. 8). On the other hand, for high permeation numbers W>>1 eq. (15) becomes:

$$C_l^{\,2}=\frac{1}{W} \qquad (19)$$

that is:

$$\frac{\sigma K_2 c_l^{\,2}}{\sigma K_2 c_{eq}^{\,2}}=\frac{\Phi}{\sigma K_1 d p_h^{\,1/2}} \qquad (20)$$

which leads to:

$$J=J_{o,l}=\sigma K_2 c_l^{\,2}=\frac{\Phi}{d}p_h^{\,1/2} \qquad (21)$$

Which is the steady-state permeation equation for a pure diffusion limited regime (eq. 7).

The solution of the general equation (15) has been evaluated numerically [18]:

$$\log\left(C_l^{\,2}\right)=\frac{\sum_{n=0}^{5} a_n\left(\ln W^2\right)^n}{\sum_{n=0}^{5} b_n\left(\ln W^2\right)^n} \qquad (22)$$

with a_0=-0.5314, a_1=-0.0927, a_2=-0.01828, a_3=-0.00126, a_4=-5.4621 10^{-5}, a_5=-8.201 10^{-7}, b_0=1, b_1=0.011, b_2=0.011295, b_3=1.7448 10^{-5}, b_4=8.9754 10^{-6}, b_5=-4.666 10^{-8}.

Figure 7 depicts this function showing how the extremes approach to pure surface or diffusion limited regimes.

4.3.2. Hydrogen transport parameters evaluation

The experiment consists of a series of permeation runs, as described in section 4.2., performed at several temperatures T within the range of interest, 523 to 723 K. At each temperature several permeation runs are carried out with different driving pressures, p_h, ranging from $5\cdot10^2$ to 10^5 Pa. As a result, the "permeation flux"-to-"driving pressure" quotient, $\frac{J}{p_h}$, is obtained for each pressure p_h and temperature T.

The solution of the general steady-state permeation equation (eq. 22) can be re-written in terms of the directly measurable data ($\left(\frac{J}{p_h}\right)$, p_h) and the unknown parameters σK_1 and Φ:

$$\log\left(\frac{J}{p_h}\right)=\log(\sigma K_1)+\frac{\sum_{n=0}^{5} a_n\left(\ln\left(\left(\frac{\sigma K_1 d}{\Phi}\right)^2 p_h\right)\right)^n}{\sum_{n=0}^{5} b_n\left(\ln\left(\left(\frac{\sigma K_1 d}{\Phi}\right)^2 p_h\right)\right)^n} \qquad (23)$$

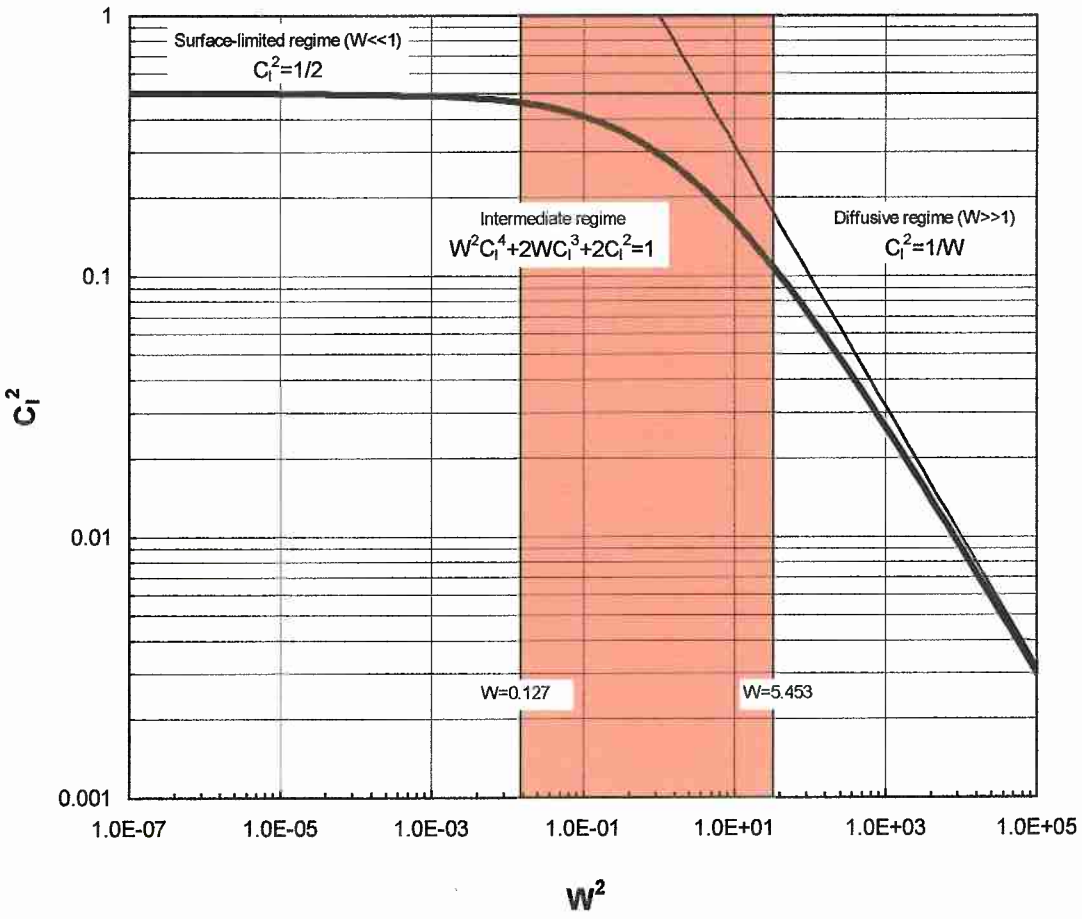

Figure 7. Graphic solution of the general equation for the steady-state permeation (eq. 15). ■ Experimented permeation number.

A non-linear least square fitting routine fits the experimental points $\left(\left(\frac{J}{p_h}\right), p_h\right)$, for each temperature, with this theoretical function (23), σK_1 and Φ being the fitting parameters.

Subsequently, a linear least square fitting routine fits the groups of previously obtained σK_1 and Φ to an Arrhenius behaviour, extracting the pre-exponentials σK_{10}, Φ_0 and the characteristic energies E_1, E_d.

E_1, the "adsorption energy", is the potential energy experimentally observed when accounting the adsorption process.

4.4. Results for permeation experiment

A series of deuterium permeation runs have been carried out in OPTIFER-IVb with H_D driving pressures p_h ranging from $5 \cdot 10^2$ to 10^5 Pa and temperatures ranging from 523 to 723 K. The results obtained are analysed in the next subsections.

4.4.1. Permeation regime definition

The first stage when analysing the obtained results is to identify the permeation regime. In Figure 8 the obtained steady-state permeation fluxes for different temperatures are depicted versus the driving pressure.

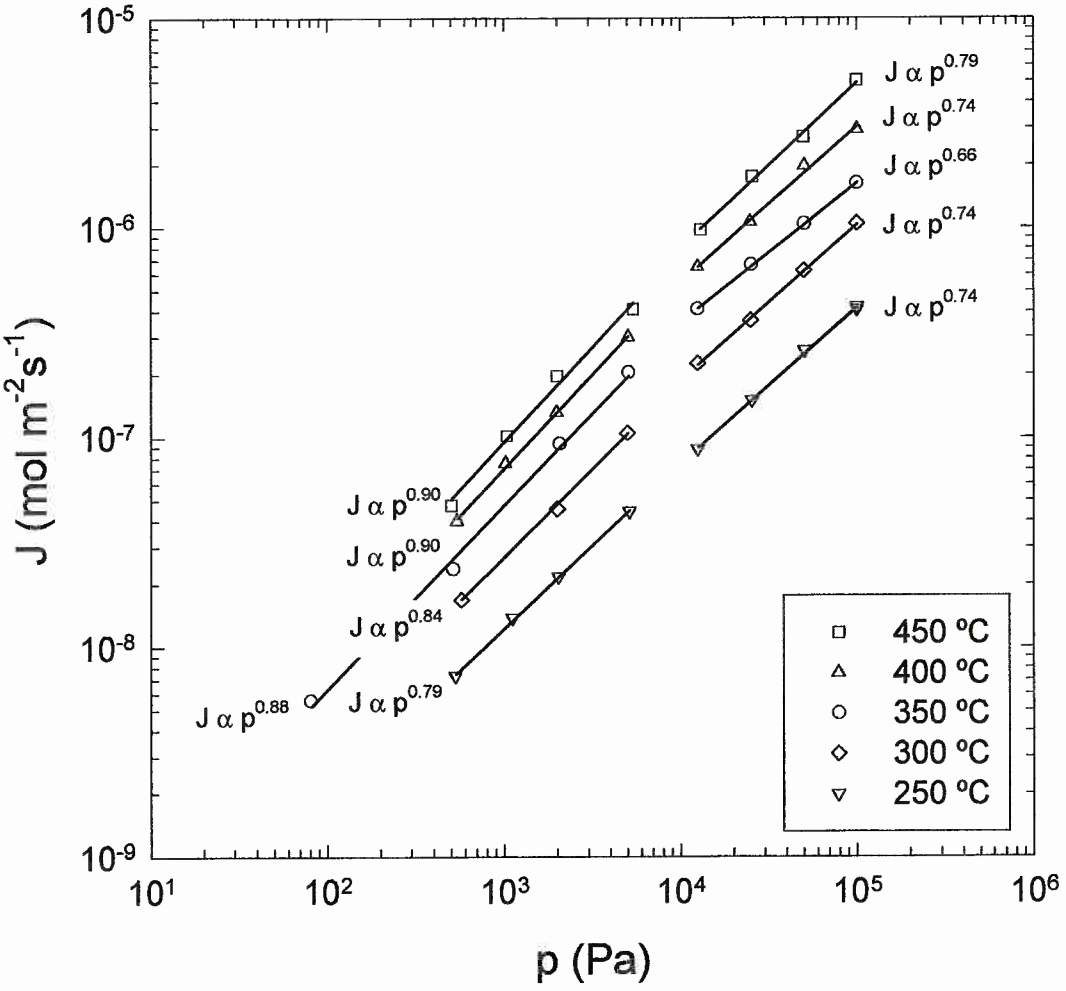

Figure 8. Steady state permeation fluxes. Transport regime characterisation.

It can be noticed that the permeation regime does not correspond to a well defined diffusion or surface limited permeation regime; because steady-state permeation fluxes follow a proportional law with a power of the driving pressure ranging from 0.90 to 0.66; i.e., it deviates from the limits 0.5 or 1. Thereby an intermediate permeation regime is evidenced. Nevertheless, it can be observed how as lower driving pressure is applied the closer the transport regime gets to a surface-limited type; i.e., the exponent of the driving pressure approximates 1. This is an evidence of how importance of surface processes grows as the H partial pressure diminishes. It must be kept in mind

that H isotopes partial pressure levels of 10^3 Pa and less are expected within the blanket of a fusion reactor blanket in nominal operating conditions.

4.4.2. Results from permeation modelling

A non-linear least square fitting routine has been applied to each group of experimental data $\left\{ \left(\frac{J}{p_h} \right)_i , (p_h)_i \right\}_T$ with eq. (23) as fitting function and σK_1 and Φ as fitting parameters. In Figure 9, a good agreement between experimental obtained results and the resultant fitting curves can be observed.

The resultant adsorption constant values are depicted together with the Arrhenius fitting in Figure 10. For H_D recombination constant evaluation H_D Sieverts' constant data (K_{s0} and E_s) from [5] have been used (Fig. 11).

The obtained surface rate constants are:

$$\sigma K_1(\text{mol m}^{-2}\text{s}^{-1}\text{Pa}^{-1}) = 2.998 \cdot 10^{-8} \exp(-29230/(RT))$$

$$\sigma K_2(\text{mol}^{-1}\ \text{m}^4\text{s}^{-1}) = 2.838 \cdot 10^{-7} \exp(28679/(RT)).$$

The obtained permeability agrees with the value obtained measuring OPTIFER-IVb by IDT in [5] (Fig. 12), the permeability obtained here is:

$$\Phi(\text{mol m}^{-1}\text{Pa}^{-1/2}\text{s}^{-1}) = 5.311 \cdot 10^{-8} \exp(-44988/(RT))$$

Once permeability Φ and adsorption constant σK_1 have been assessed, the permeation number W can be evaluated (Table 3). It is remarkable the fact that all the permeation numbers range from 0.127 to 5.453; these values can not be considered either $W \gg 1$ or $W \ll 1$, concluding that the intermediate transport regime is the proper one to be recognised, rather than pure surface-limited or diffusion-limited regimes (Fig. 7).

From Table 3 it is evidenced that the permeation number diminishes as the driving pressure is lowered and the experimental temperature increases. As a consequence, the surface effects for OPTIFER-IVb become more important in H transport

characterisation not only when H experimental pressure level is lower, but, simultaneously, when the experimental temperature is higher.

The theoretical definition of the permeation number agrees with this experimentally obtained dependence of the driving pressure p_h and temperature T; W diminishes with lower p_h because it is proportional to its square root, and it diminishes with higher T because it is activated with a resultant energy (E_I-E_s-E_d) that has turned out to be negative, -15758 $J \cdot mol^{-1}$.

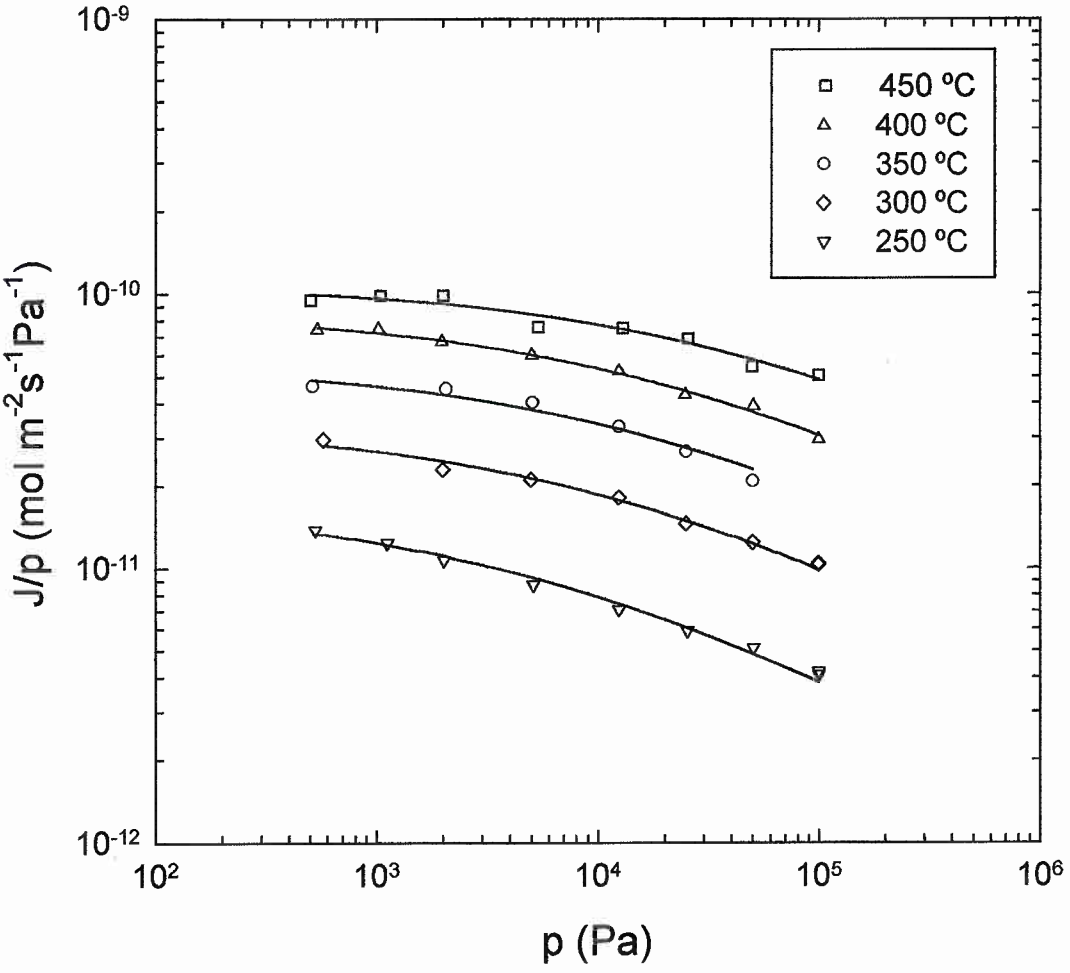

Figure 9. Fitting curves for permeation experimental results.

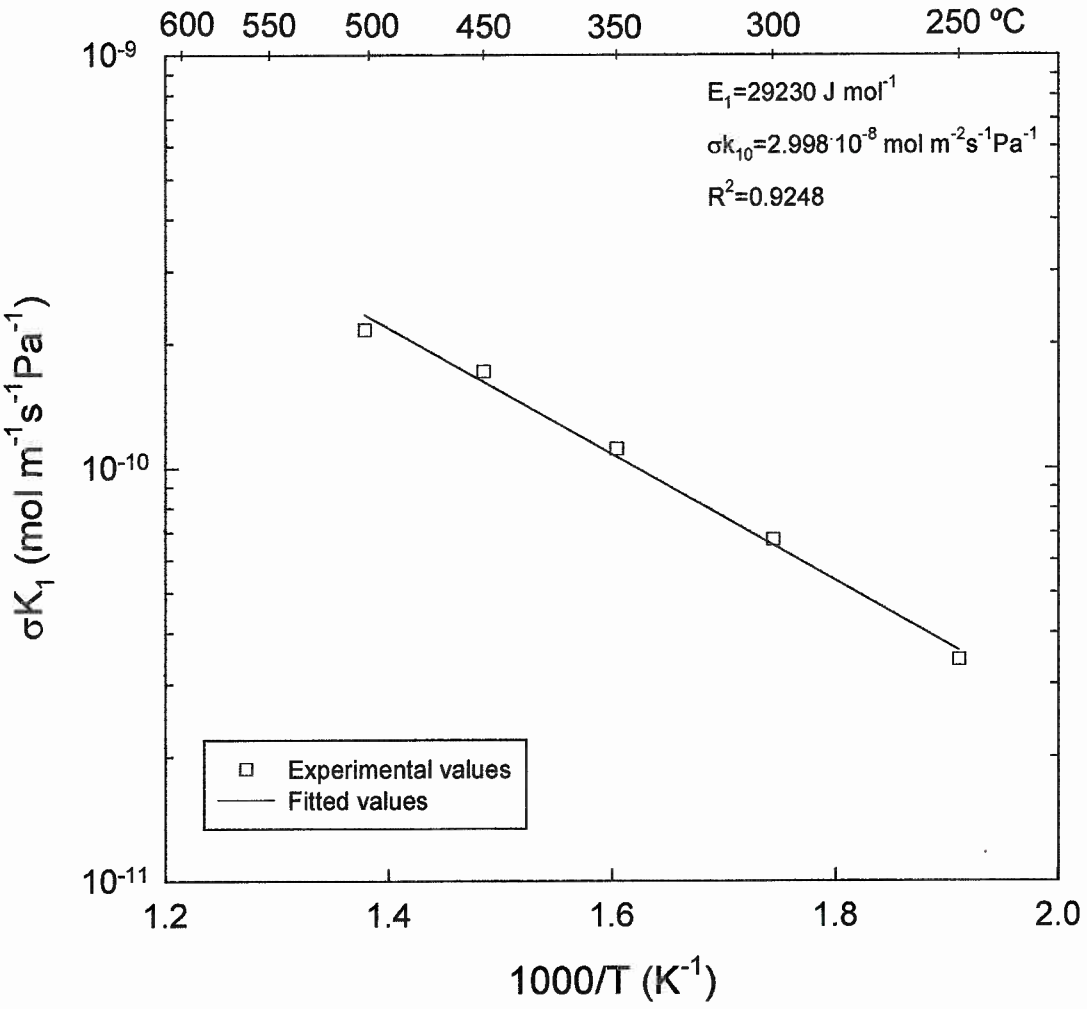

Figure 10. Arrhenius plot of the fitted adsorption constant (PT).

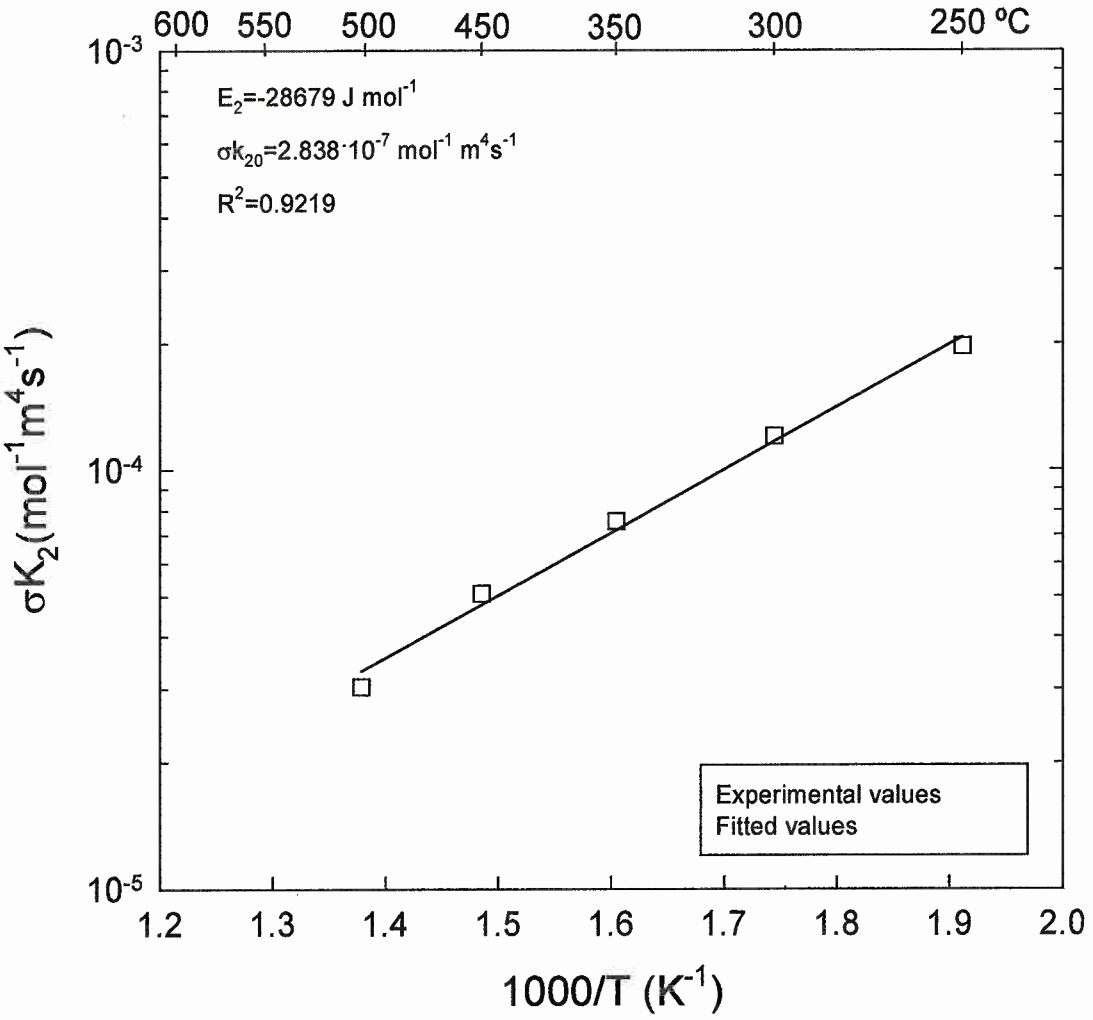

Figure 11. Arrhenius plot of the fitted recombination constant (PT).

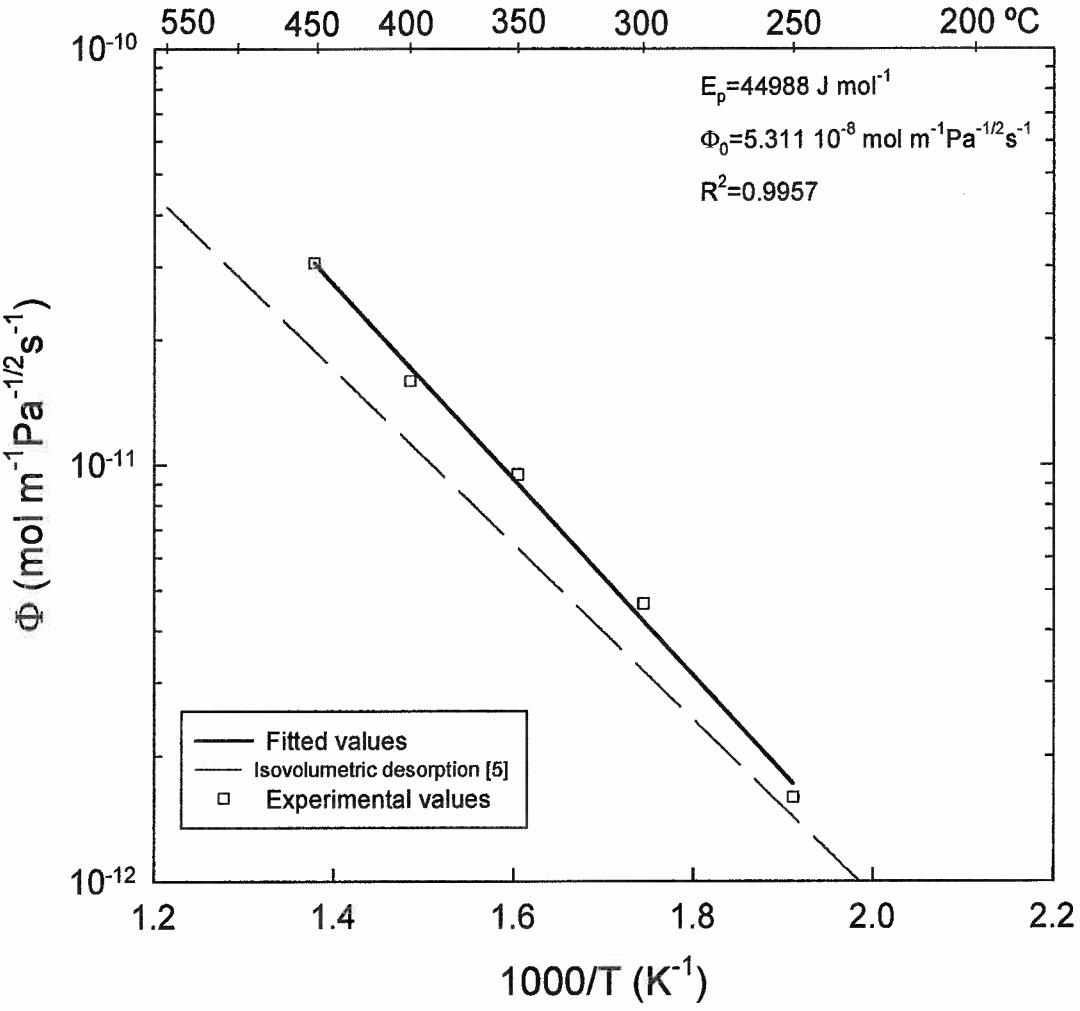

Figure 12. Arrhenius plot of the fitted permeability (PT).

Table 3. Derived permeation numbers (W).

		T (°C)				
		450	**400**	**350**	**300**	**250**
p_h (Pa)	10^5	1.792	2.727	-	3.664	5.453
	$5\ 10^4$	1.267	1.940	2.11	2.592	3.878
	$2.5\ 10^4$	0.907	1.362	1.492	3.662	2.752
	$1.25\ 10^4$	0.647	0.964	1.052	1.831	1.929
	$5\ 10^3$	0.416	0.613	0.670	1.295	1.235
	$2\ 10^3$	0.253	0.384	0.428	0.819	0.777
	10^3	0.182	0.275	-	0.518	0.576
	$5\ 10^2$	0.127	0.201	0.213	0.277	0.397

5. ISOVOLUMETRIC DESORPTION EXPERIMENT

5.1. The isovolumetric desorption facility

A schematic view of the IDT rig is shown in Figure 13. This installation and the procedure for a IDT measurement has been exhaustively described in earlier reports [5, 6].

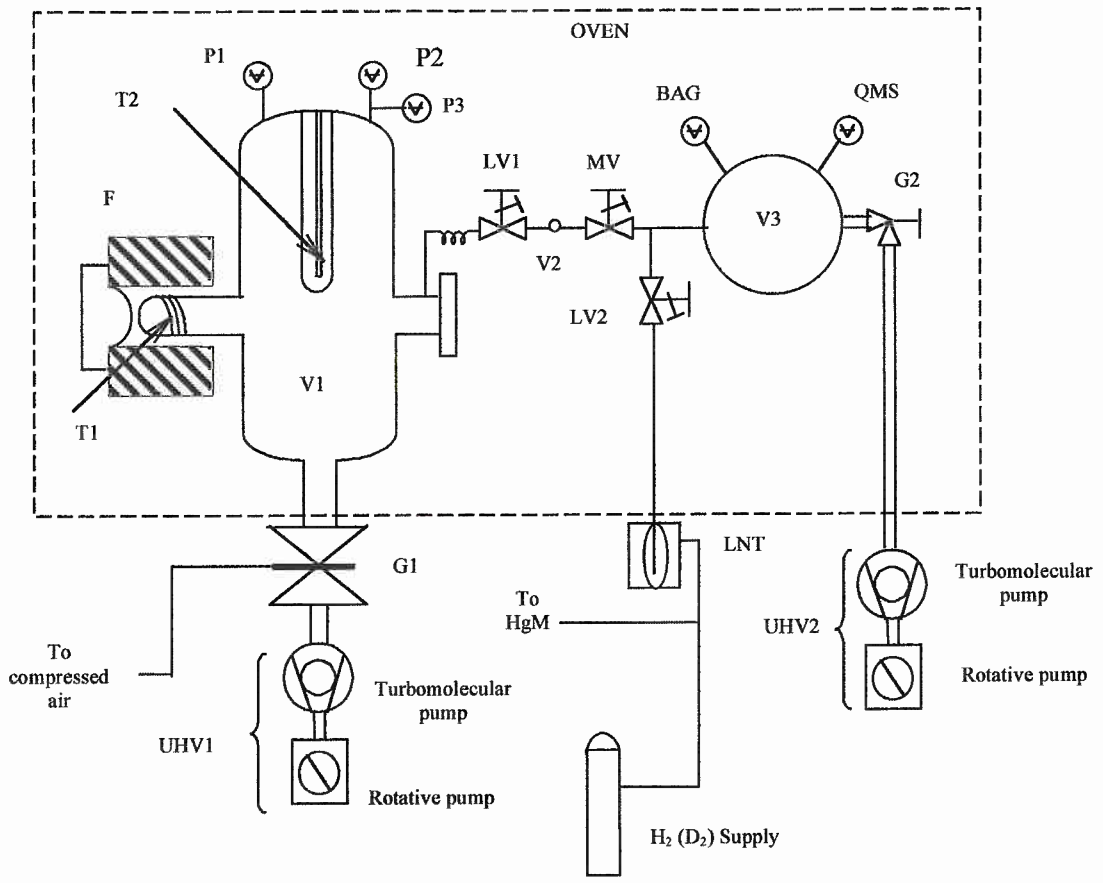

BAG	Bayard-Alpert Gauge	MV	Manually actuated magnetic valve
F	Furnace	P1, P2	Capacitive manometers
G1	Electropneumatic gate valve	P3	Spinning rotor gauge
G2	Manually actuated gate valve	QMS	Quadrupole mass spectrometer
HgM	U-tube Hg manometer	T1, T2	Pt-Resistance Thermometers
LNT	Liquid Nitrogen Trap	UHV	Ultra high vacuum pumping units
LV1,2	Manually actuated leak valves	V1	Experimental chamber
		V2, V3	Expansion volumes

Figure 13. Schematic view of the isovolumetric desorption facility.

The IDT rig comprises ultra high vacuum stainless steel components, such as the gate valves for the turbomolecular pumps (G1 and G2), the manually actuated leak valves (LV1 and LV2) and extensive pipe-work. It also has volumes in Pyrex glass, a temperature resistant material that reduces the background H pressure by outgassing from the experimental chamber (V1).

The ultra high vacuum is obtained by two pumping units (UHV1 and UHV2) similar to the PT rig ones.

The specimens are placed into the nozzle of the experimental chamber (V1), where a resistance furnace (F) provides the heat needed to operate over the entire range of the measurement temperatures. The furnace temperature is controlled by two nickel/ /chromium-nickel thermocouples. Two Pt-resistance thermometers (T1 and T2) register the specimen and the experimental chamber temperature, respectively.

The evolution of the H from the specimens is recorded by measuring the pressure change in the containing chamber (V1). A capacitance manometer (P1) covering the pressure range from from 1 to 10^5 Pa, measures the pressure when charging the specimens with gas; whereas another capacitance manometer (P2) covering the pressure range from 10^{-3} up to 10^2 Pa and a spinning rotor gauge (P3) measure the pressure rise during the release phase.

The expansion volume (V3), the Bayard-Alpert Gauge (BAG), and the Quadrupole Mass Spectrometer (QMS) constitute the gas analysing unit. This unit would detect the possible presence of deleterious components in the measurement chamber.

5.2. The isovolumetric desorption experimental procedure

A single IDT run consists of recording the pressure increase in the vessel V1 due to outgassing from the specimen, which has been previously loaded with H at a given pressure and temperature. During the loading phase the gas concentration in the specimen builds up until equilibrium with the external pressure is reached. A quick,

but thorough, pumping down of the vessel V1 breaks this equilibrium, starting the gas release from the material.

The volume of the experimental chamber (V1), where the H released from the specimens is contained, has been accurately calculated by an expansion into a calibrated volume (Sieverts' method). The measured effective volume V1 is $5.491 \cdot 10^{-6}$ m^{-3}. The knowledge of this volume permits the conversion of the measured pressure increase into an effective amount of released H, or an effective H diffusive flux through the specimen surface at every moment of the desorption phase.

Each measurement is followed by a blank run, under the same experimental conditions, (i.e. same loading pressure and temperature), without specimens, to account for the contribution of the inner wall outgassing of the vessel V1. The "net" pressure release curve is obtained then by point-to-point pressure subtraction (Fig. 14).

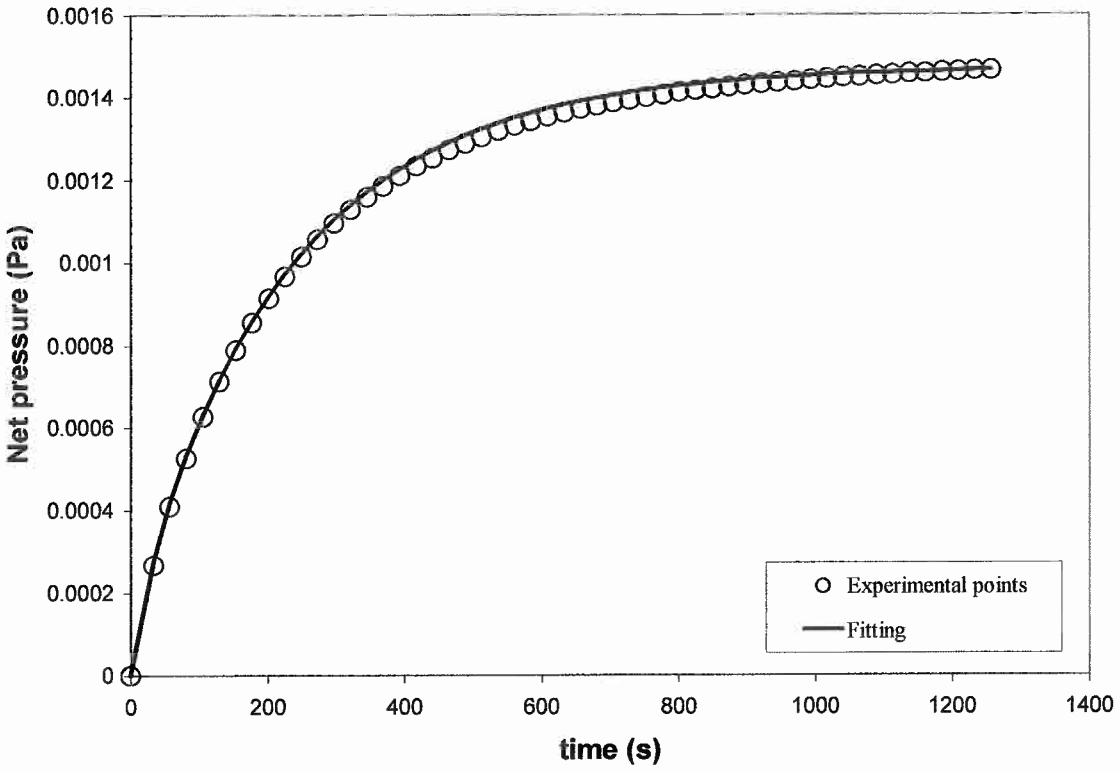

Figure 14. Experimental result of IDT pressure increment and fitting.

A non-linear least squares fitting to the experimental net pressure release curve gives the Sieverts' constant and the surface rate constants σK_1 and σK_2 for each experimental condition.

5.3. Isovolumetric desorption modelling

5.3.1. Surface-limited transport regime

The theoretical applied model analyses the surface-limited transport regime; i.e. hydrogen transport is limited by physico-chemical reactions occurring at the surface. All bulk processes are assumed to happen instantaneously compared to the time scale of surface reactions, so that any concentration gradient is cancelled by diffusion at each time; the concentration c may be treated as uniform inside the specimen, that is $c(r,t)=c(t)$. That is why the model developed hereafter is dependent of the surface area without any connection with the geometrical shape of the specimen.

This surface-limited model allows evaluation of the surface rate constants, σK_1 and σK_2, and the Sieverts' constant K_s. The IDT studies the H release from a previously up-to-saturation loaded cylinder of material kept at constant temperature.

A surface-limited transport regime has been developed for modelling IDT runs when transport is limited by the surface reactions adsorption and recombination [20]. Here we will briefly develop the model for its better understanding.

First, the continuity equation must be taken into account:

$$\left(\frac{V}{RT}\right)\frac{dp(t)}{dt} + V_s\frac{dc(t)}{dt} = 0 \qquad (24)$$

p being the pressure in the measurement chamber (V1), V and T the chamber volume and temperature, respectively. R is the ideal gas' constant, V_s the specimen volume and c(t) the H concentration in the specimen. This equation indicates that an increment in the chamber gas pressure is due to a decrease in the concentration of the gas dissolved in the specimen.

The initial condition is set at the beginning of the pumping-down phase, just a short time before the release phase begins:

$$c(0) = c_i = K_s\sqrt{p_i} \tag{25}$$

p_i being the H loading pressure and c_i the initial H concentration. Where Sieverts' law has been assumed to be fulfilled because a long enough loading time for reaching a saturation state has been taken. The solution of equation (24) with this initial condition becomes:

$$p(t) + \Delta p = RT\frac{V_s}{V}(c_i - c(t)) \tag{26}$$

where Δp accounts for the H pressure increment lost during the pump-down phase. Eq. (26) can be expressed in a more simple way:

$$p(t) = p_c - RT\frac{V_s}{V}c(t) \tag{27}$$

with $p_c = RT\frac{V_s}{V}c_i - \Delta p$.

Equating the dissolved gas diminution with the amount of gas passing throughout the surface of the material, the following expression is obtained:

$$V_s\frac{dc(t)}{dt} = A_s\left(\sigma K_1 p(t) - \sigma K_2 c(t)^2\right) \tag{28}$$

A_s being the geometrical area of the specimen.

Considering eqs. (27) and (28) the general differential equation for a surface-limited regime in a IDT experiment is derived:

$$\frac{dc(t)}{dt} = -\sigma K_2\frac{A_s}{V_s}c(t)^2 - \sigma K_1\frac{A_s RT}{V}c(t) + \sigma K_1\frac{A_s}{V_s}p_c \tag{29}$$

The solution of equation (29), i.e. Ricatti's equation:

$$\frac{dc}{dt} = Lc^2 + Mc + N \tag{30}$$

is the following:

$$c(t) = c_f + \frac{(c_i - c_f)(M + 2Lc_f)}{(M + L(c_i + c_f))\exp(-(M + 2Lc_f)t) - L(c_i - c_f)} \tag{31}$$

where

$$c_f = \frac{V_s RT}{2V}\frac{\sigma K_1}{\sigma K_2}\left(\sqrt{1+4\frac{V^2 \sigma K_2 p_c}{V_s{}^2 \sigma K_1 (RT)^2}}-1\right) \tag{32}$$

is the final concentration. By substituting eq. (31) for c(t) in eq. (27), the pressure law

$$p(t) = p_f + (p_f + \Delta p)\frac{\left[1+p_c\frac{\sigma K_2}{\sigma K_1}\left(\frac{2V}{V_s RT}\right)^2\right]^{1/2}}{\frac{\sigma K_2 V}{\sigma K_1 V_s RT}(c_i - c_f) - \left[1+\frac{\sigma K_2 V}{\sigma K_1 V_s RT}(c_i + c_f)\right]\exp\left(\frac{t}{\tau_s}\right)} \tag{33}$$

is obtained, where the surface release characteristic time τ_s has been defined by:

$$\tau_s = \frac{-1}{M + 2Lc_f} = \frac{V}{A_s RT \sigma K_1}\left[1+p_c\frac{\sigma K_2}{\sigma K_1}\left(\frac{2V}{V_s RT}\right)^2\right]^{-1/2} \tag{34}$$

These expressions, eq. (33) and (34) will be used in the IDT modelling that is explained in the next subsection.

5.3.2. Surface rate constants evaluation

The solution of the general differential equation for a surface-limited regime in IDT experiment, eq. (33), can be rewritten in a more simple way as:

$$p(t) = p_f + \frac{p_f + \Delta p}{U - (U+1)\exp\left(\frac{t}{\tau_s}\right)} \tag{35}$$

with

$$U = \frac{(p_f + \Delta p)\left(\frac{V}{K_s V_s RT}\right)^2}{1+\frac{2V}{K_s V_s RT}\sqrt{p_f}} \tag{36}$$

where an equivalent expression for τ_s is

$$\tau_s = \frac{V}{A_s RT \sigma K_1}\left(1+\frac{2V\sqrt{p_f}}{K_s V_s RT}\right)^{-1} \tag{37}$$

Taking into account Sieverts' law at the end of the loading and release phases

$$K_s = \frac{c_i}{\sqrt{p_i}} = \frac{c_f}{\sqrt{p_f}} \tag{38}$$

and that eq. (26) for $t \to \infty$ becomes

$$p_f + \Delta p = RT \frac{V_s}{V}(c_i - c_f) \tag{39}$$

Sieverts' constant can be expressed as function of directly measured parameters and the only unknown Δp:

$$K_s = \frac{(p_f + \Delta p)\frac{V}{RTV_s}}{\sqrt{p_i} - \sqrt{p_f}} \tag{40}$$

Therefore, substituting (40) in (36) the U parameter can be expressed as function of directly measured parameters and the only unknown Δp.

A non-linear least square fitting routine fits the experimental net pressure release curve with the theoretical function (35), Δp and τ_s being the only unknown fitting parameters. From the obtained Δp and τ_s in each fitting, the Sieverts' constant K_s and the surface rate constants σK_1 and σK_2 are derived for each experimental condition (p_i, T_i) using eq. (40), (37) and (3).

5.4. Results for isovolumetric desorption experiment

The experiment consists of a series of runs composed, each one, by loading, pump-down and release phases, as described in section 5.2., performed at several temperatures T within the range of interest, 553 to 903 K. At 745 K several IDT runs are carried out with different loading pressures, p_i, from $4 \cdot 10^4$ to 10^5 Pa, in order to assess the class of transport regime. The results obtained are analysed in the next subsections.

5.4.1. Transport regime

The loading-release runs done at 745 K with several H_P loading pressures 10^5, $8 \cdot 10^4$, $6 \cdot 10^4$ and $4 \cdot 10^4$ Pa lead to net pressure release curves that, after having been normalised with the loading final pressure, are depicted in Figure 15.

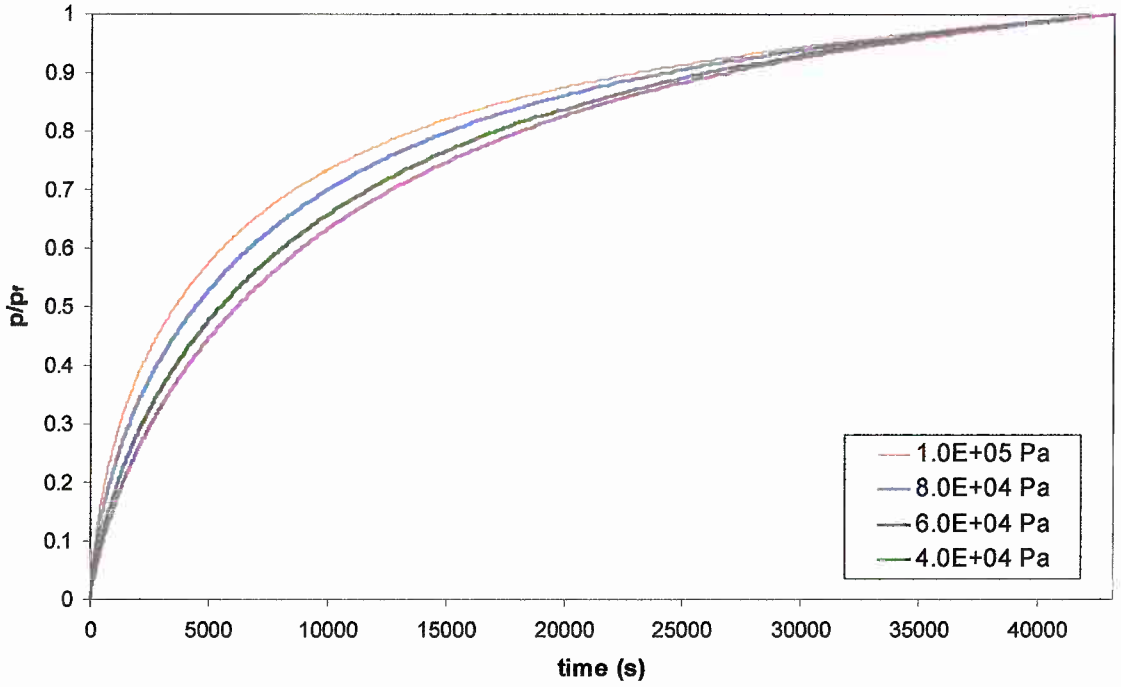

Figure 15. Normalised pressure release curves undertaken at the same temperature (745 K) at different pressures.

From this set of four measurements it can be noticed how the higher the loading pressure the faster the kinetic is. When a diffusive regime occurs transport kinematics are not affected by the loading pressure level and normalised pressure release curves for different pressures and the same temperature overlap, as it was reported in [6].
As a result, a surface-limited regime has been considered here. The results coming from the modelling of the pressure release curves in this class of transport regime are analysed in the next subsection.

5.4.2. Results from isovolumetric desorption modelling

A non-linear least square fitting routine has been applied to each net pressure release curve using equations (35), (36), (37) and (40) with Δp and τ_s as fitting parameters.

From these values and using equations (40), (37) and (3), the parameters of interest σK_1, σK_2 and K_s are directly evaluated.

The resultant H_P adsorption and recombination constant values are depicted in Figures 16 and 17, together with the results for H_D obtained using the PT.

It can be noticed that the experimental values of the surface constants σK_1 and σK_2 are all much below the expected ones when considering the tendency showed by the PT-derived constants. Furthermore it is impossible to fit these values, over the complete experimental temperature range, to an Arrhenius law with a reasonable quality.

The reason of the dispersion of data obtained by IDT may be reported as a progressive change in the specimens' surface condition undergone between the loading-release runs, wherein an oxide layer has been continuously building up. As a consequence, the sticking coefficient has been diminishing as that oxide layer grew; leading to an effective reduction of the experimental surface rate constant values.

If the main surface change due to oxidation is assumed to happen during the rising temperature period, i.e., during the first four experimental runs, fitted surface constants (for experimental values (4)-(9)) may be derived (Figures 16 and 17). The activation energies for surface constants obtained in his manner, 29201 $J \cdot mol^{-1}$ for E_1 and –14269 $J \cdot mol^{-1}$ for E_2, are similar to those obtained in the PT experiment, E_1=29230 $J \cdot mol^{-1}$ and E_2=-28679 $J \cdot mol^{-1}$; the parallel displacement accounted, with respect to PT surface constants, is due to different pre-exponential constants that may be attributed to diverse sticking coefficients, s, for each specimen surface.

An X-ray Photoelectron Spectroscopy (XPS) and a Scanning Electron Microscopy (SEM) of the specimens surface carried out at the end of the IDT experiment have reported the existence of an oxide layer of width 2 μm in average, composed essentially by Cr_2O_3 and manganese oxides MnO_x, or a combination of both (spinel:$Cr_xMn_yO_4$); presence of iron oxides, FeO_x, were detected too (Figure 18).

In Figure 19 the Sieverts' constant derived in the present IDT experiment is depicted together with that reported for OPTIFER-IVb in [6], where a clean specimens surface was assured during all the experiment. It is worth noting that the first obtained value of Sieverts' constant, (1), agrees very well with the curve derived for clean specimens [6]; from then on, the experimental Sieverts' constant values have increased in relation to the expected ones, departing further from them as the run continues in time (note the sequence number in the graph). This may be recognised as the effect of oxide layer widening, because it is well known the high H solubility of steel oxides [21].

In relation with this matter a two regions (steel-oxide) diffusive H transport regime will be analysed in the future, from which the thickness and H transport parameters of the oxide will be able to be obtained.

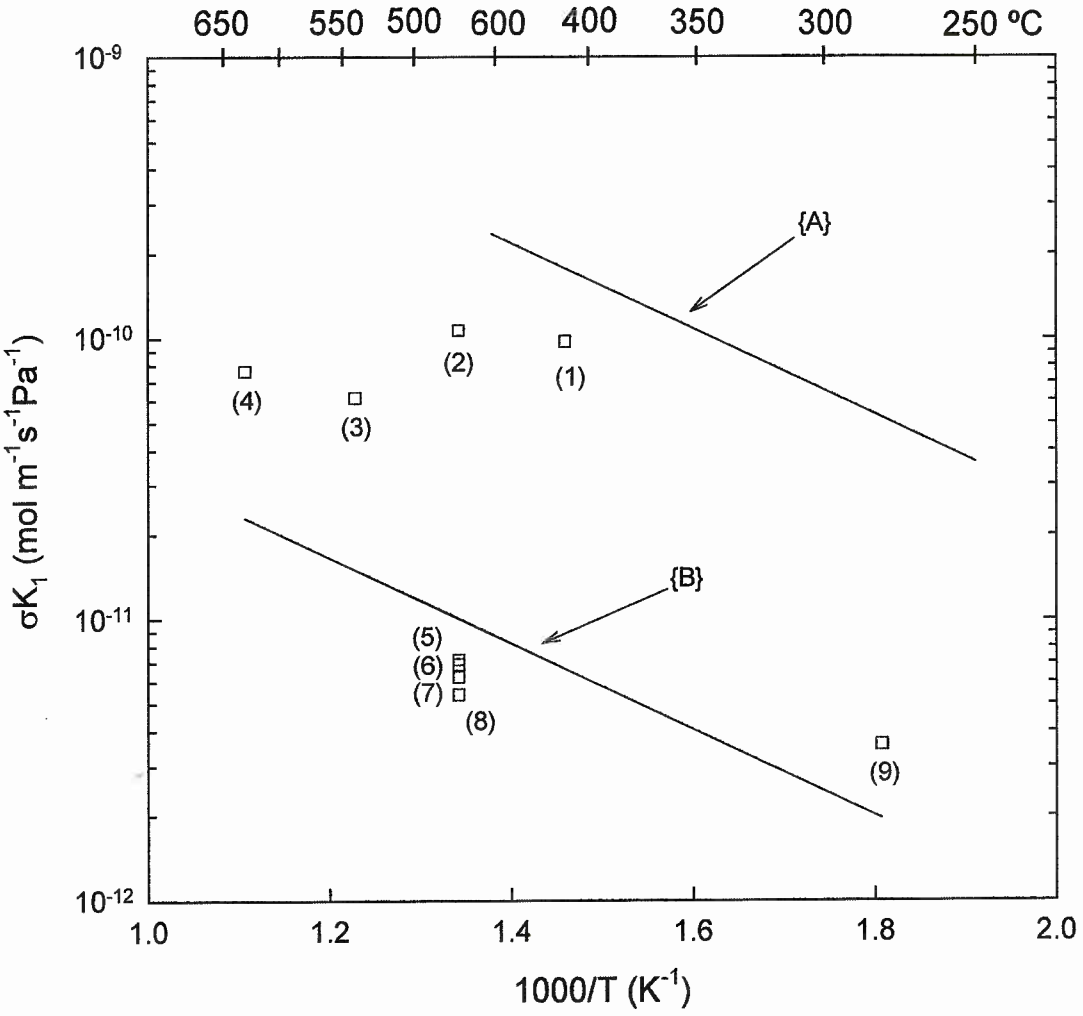

Figure 16. Arrhenius plot of the adsorption constant values. The number in parenthesis indicates the order of measurement. {A} permeation technique; {B} Isovolumetric desorption technique, fitting to (4)-(9) experimental points.

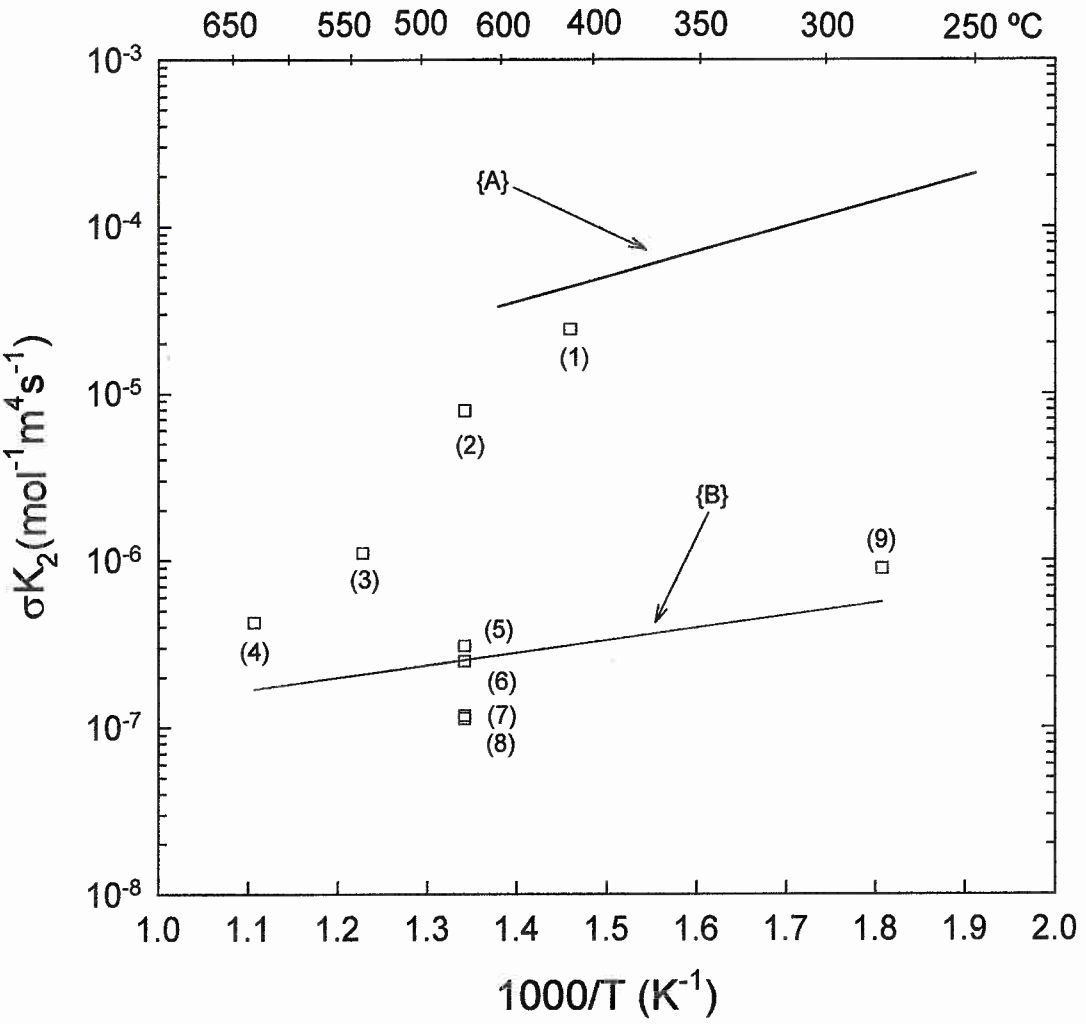

Figure 17. Arrhenius plot of the recombination constant values. The number in parenthesis indicates the order of measurement. {A} permeation technique; {B} Isovolumetric desorption technique, fitting to (4)-(9) experimental points.

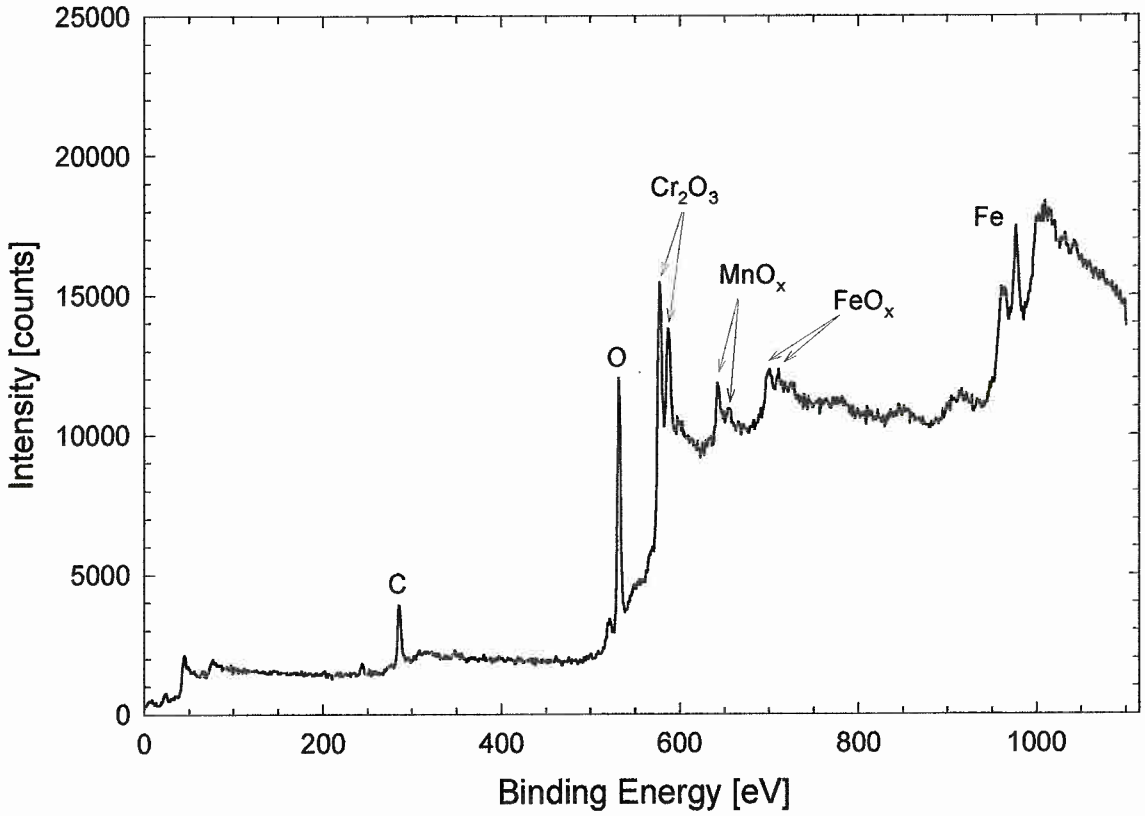

Figure 18. XPS spectrum of oxidised OPTIFER-IVb, showing the presence of Mn, Cr and Fe oxides.

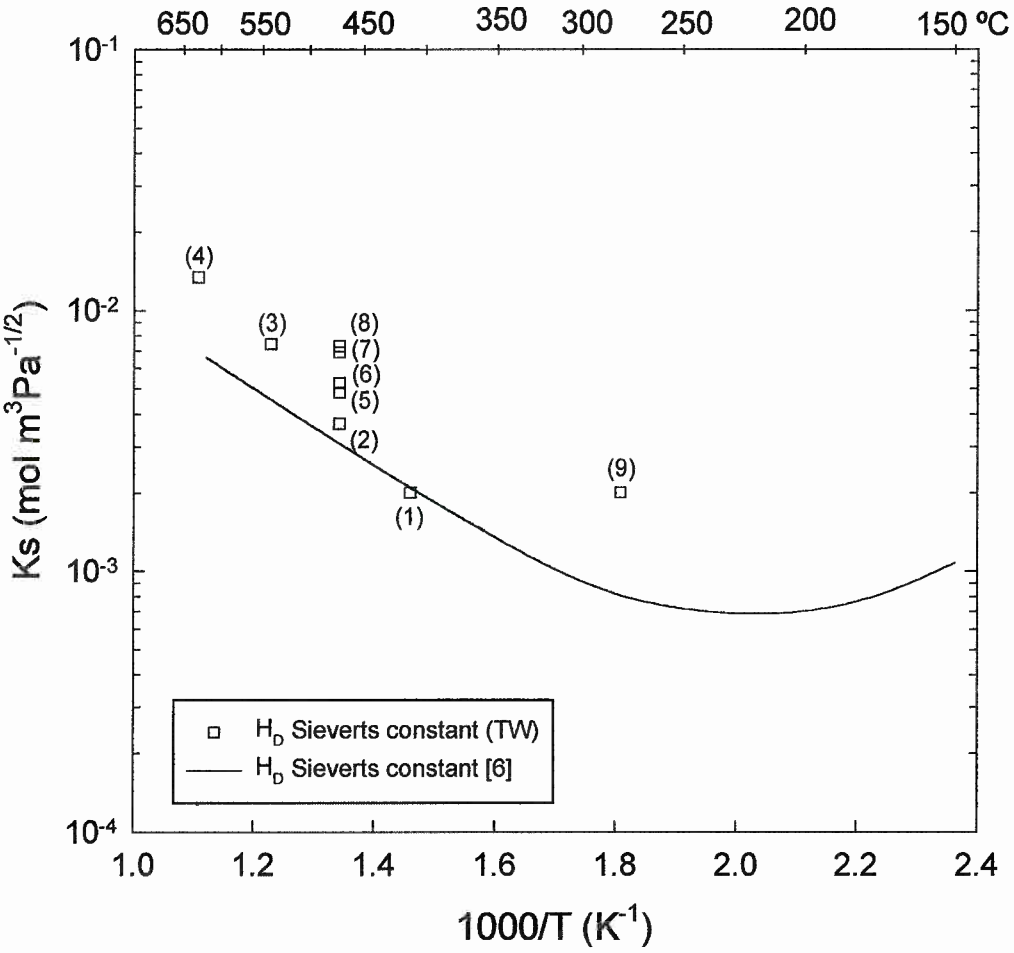

Figure 19. Arrhenius plot of the Sieverts' constant values (IDT). The number in brackets indicates the order of measurement.

6. COMPARISON OF RESULTS

The surface rate constants derived using IDT and PT are depicted in Figures 20 and 21 together with the values theoretically derived using Baskes and Pick & Sonnenberg models for OPTIFER-IVb with roughness σ=1 and sticking probability s=1. Some experimental surface rate constants corresponding to other stainless steels are included for comparison.

The surface rate constant values obtained using IDT are significantly affected by a progressive surface oxidation. That is why the σK_1 and σK_2 values are lower than the ones evaluated by means of PT and have not been able to be fitted properly to an Arrhenius tendency.

The surface rate constants σK_1 and σK_2 obtained by means of PT are close to those of MANET in [17]. The value of the activation energy of the adsorption constant, σK_1, for the Baskes model is 40276 J mol^{-1}; this value is acceptably close (27% of deviation) to our directly estimated value of 29230 J mol^{-1}. The difference between the Baskes' model σK_1 and the adsorption constant measured by PT can be explained focusing on the real surface conditions; i.e., the real surface may present a certain roughness bigger than the ideal value, σ>1, and the sticking probability may diminish if the specimen surface is not perfectly absent of metallic oxides, s<1. A value of the product $\sigma \cdot s = 1.185 \cdot 10^{-7}$ explains the difference between the result experimentally obtained and the theoretical value obtained with Baskes model.

The Pick and Sonnenberg model yields a σK_1 constant without an activation energy which disagrees with our experimental result; an activation energy of $2E_C$=29230 in the sticking coefficient may explain that difference.

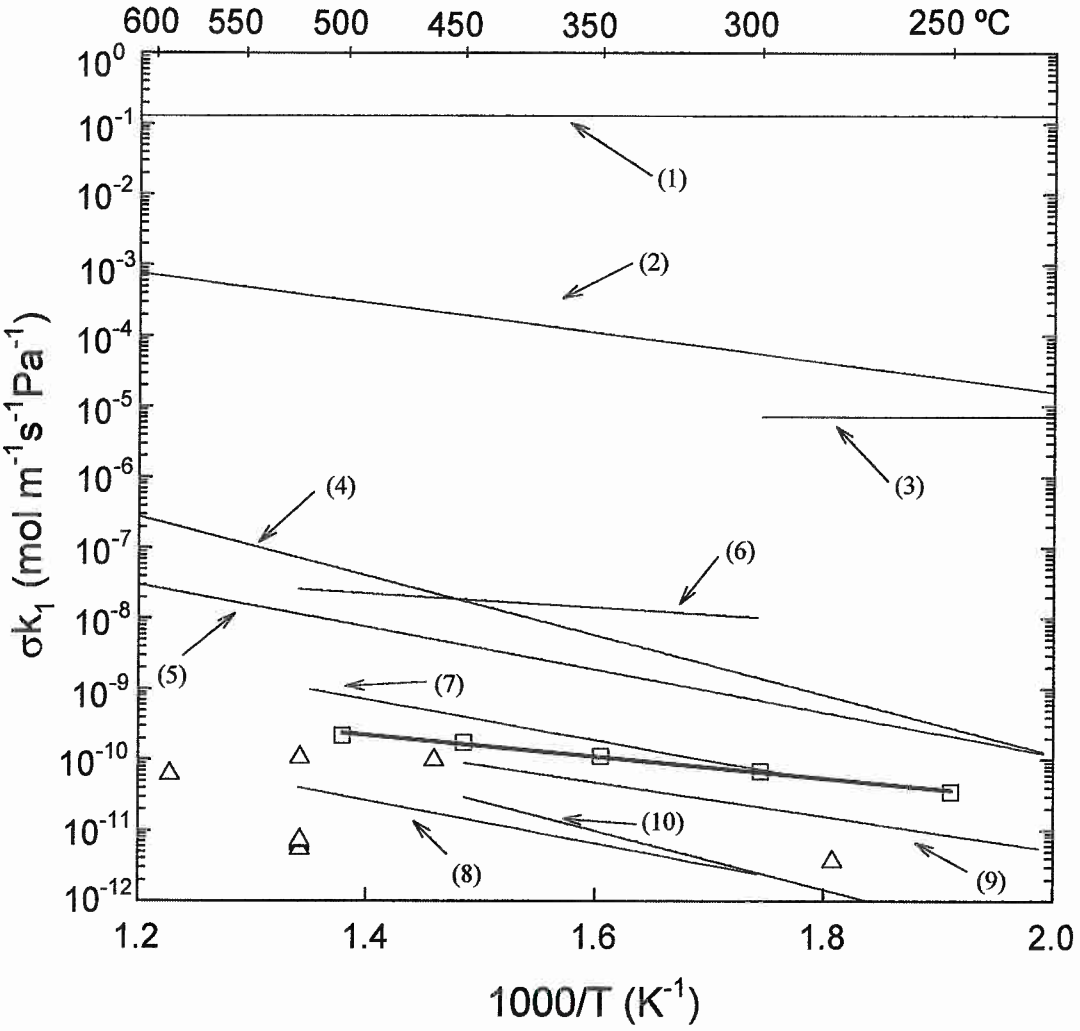

Figure 20. Arrhenius plot of adsorption rate constants. The triangled points are the experimental adsorption rate constant values obtained by IDT, the squared ones the experimental adsorption rate constant values obtained by PT. Another referenced values are included for comparison: (1) and (2) Pick & Sonnenberg [14] model and Baskes [13] model respectively for OPTIFER-IVb (with sticking coefficient s=1 and roughness σ=1); (3) D^+ implantation in MANET [22]; (4) H_2, 316 SS ion beam cleaned [23], (5) H_2, 316 SS oxidized both surfaces [23], (6) D_2, bare MANET [18]; (7) D_2, MANET [17], (8) D_2, oxidized MANET [18]; (9) D_2, Inconel 600 [24], (10) D_2, 304 SS [25].

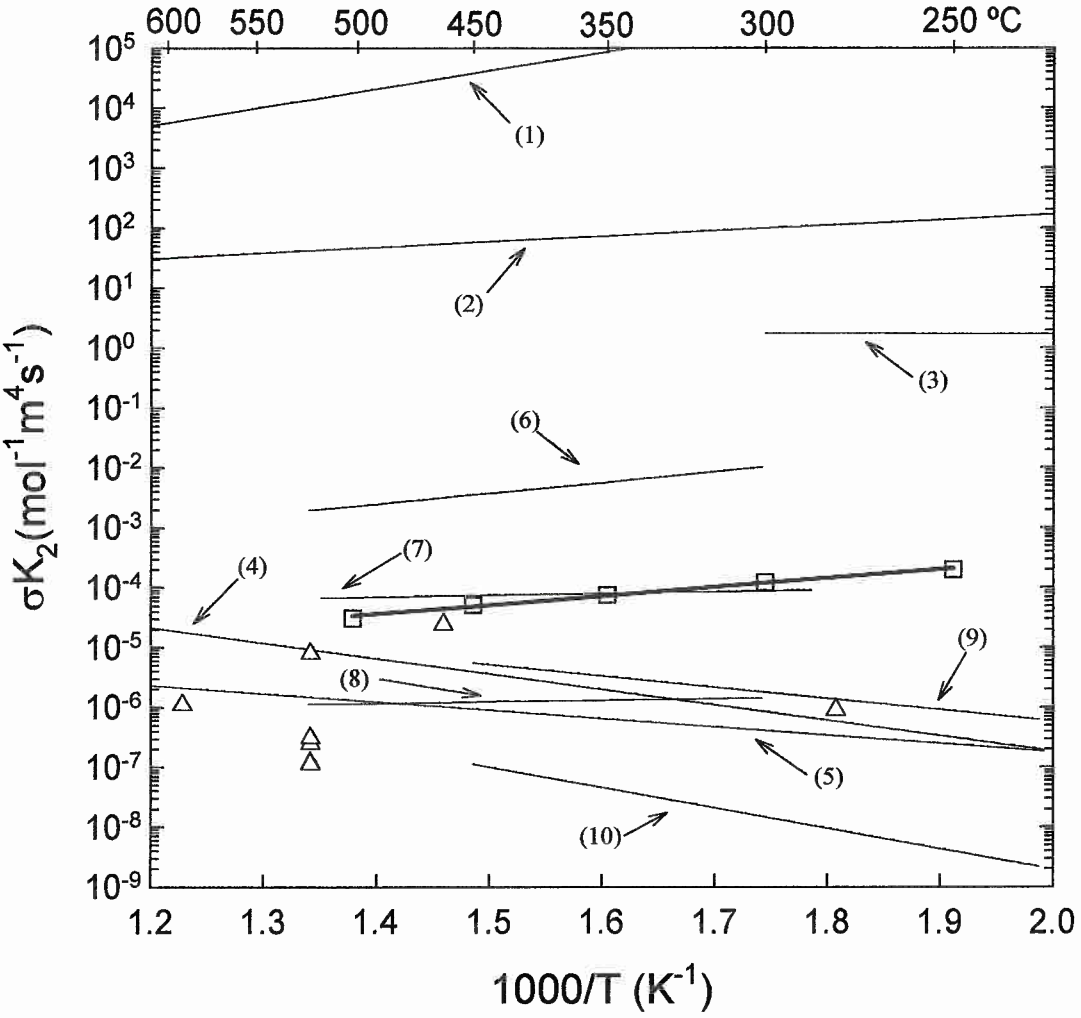

Figure 21. Arrhenius plot of recombination rate constants. The triangled points are the experimental adsorption rate constant values obtained by IDT, the squared ones the experimental adsorption rate constant values obtained by PT. Another referenced values are included for comparison: (1) and (2) Pick & Sonnenberg [14] model and Baskes [13] model respectively for OPTIFER-IVb (with sticking coefficient s=1 and roughness σ=1); (3) D^+ implantation in MANET [22]; (4) H_2, 316 SS ion beam cleaned [23], (5) H_2, 316 SS oxidized both surfaces [23], (6) D_2, bare MANET [18]; (7) D_2, MANET [17], (8) D_2, oxidized MANET [18]; (9) D_2, Inconel 600 [24], (10) D_2, 304 SS [25].

7. CONCLUSIONS

Two gas evolution techniques have been used to obtain the hydrogen surface rate constants, adsorption σK_1 (mol $m^{-2}s^{-1}Pa^{-1}$) and recombination σK_2 ($mol^{-1}m^4s^{-1}$), in the martensitic steel OPTIFER-IVb, an European candidate martensitic steel manufactured to be employed as a blanket structural material of a future thermonuclear reactor. The permeation technique was carried out over a temperature range of 523 to 723 K with a deuterium driving pressure ranging from $5 \cdot 10^2$ to 10^5 Pa, whereas the isovolumetric desorption technique was carried out over a temperature range of 553 to 903 K with a protium driving pressure ranging from $4 \cdot 10^4$ to 10^5 Pa.

The deuterium surface rate constants derived are:

$$\sigma K_1(\text{mol } m^{-2}s^{-1}Pa^{-1}) = 2.998 \cdot 10^{-8} \exp(-29230/(RT))$$

$$\sigma K_2(mol^{-1}m^4s^{-1}) = 2.838 \cdot 10^{-7} \exp(-28679/(RT))$$

The deuterium permeability has been derived in the permeation technique showing a complete agreement with the deuterium diffusive transport parameters previously measured using the isovolumetric desorption experiment. The H_D permeability derived here is:

$$\Phi(\text{mol } m^{-1}Pa^{-1/2}s^{-1}) = 5.311 \cdot 10^{-8} \exp(-44988/(RT))$$

The permeation number W for OPTIFER-IVb is activated with a negative energy equalling -15758 $J \cdot mol^{-1}$; therefore, besides low H pressures, high temperatures make surface effects in OPTIFER-IVb becoming more determinant when characterising H transport.

A progressive change in the specimens surface condition due to an oxide layer built-up has been evidenced in the isovolumetric desorption experiment. As a consequence, a diminution of the effective surface rate constant values and an increase of Sieverts' constant values have been noticed. Further analysis in H transport within the steel oxide is required; characterising H transport parameters in oxide will be the aim of a future work where a two-region diffusive H-transport model will be considered.

8. REFERENCES

[1] K. S. Forcey, I. Iordanova, M. Yaneva, J. Nucl. Mater. 240 (1997) 118.

[2] E. Serra, A. Perujo, G. Benamati, J. Nucl. Mater. 245 (1997) 108.

[3] L. Schäfer, M. Schirra, K. Ehrlich, J. Nucl. Mater. 233-237 (1996) 264.

[4] K. Ehrlich, S. Kelzenberg, H.-D. Röhrig, L. Schäfer, M. Schirra, J. Nucl.

[5] G.A. Esteban, L.A. Sedano, A. Perujo, K. Douglas, B. Mancinelli, P.L. Ceroni, G.B. Cueroni in: "Isotope Effects in Hydrogen Transport Parameters in the Martensitic Steel OPTIFER-IVb", EUR 19021 EN, 1999.

[6] G.A. Esteban, L.A. Sedano, A. Perujo, K. Douglas, B. Mancinelli, P.L. Ceroni, G.B. Cueroni in: "Hydrogen transport parameters and trapping effects in the martensitic steel OPTIFER-IVb", EUR 18995 EN, 1999.

[7] K.J. Dietz, F. Waelbroeck and P. Wienhold, Jül-1448 (1997).

[8] M.I. Baskes, SAND 83-8231 (1983).

[9] P. Wienhold, M. Profant, F. Waelbroeck and J. Winter, Jül-1825 (1983).

[10] G. Gervasini and F. Reiter, J. Nucl. Mater. 155-157 (1988) 754.

[11] A. Perujo, K. Douglas, E. Serra, Fus. Eng. Design 31 (1995) 101.

[12] P. M. Richards, J. Nuc. Mater. 152 (1988) 246.

[13] M.I. Baskes, J. Nuc. Mater. 92 (1980) 318.

[14] M.A. Pick and K. Sonnenberg J. Nuc. Mater. 131 (1985) 208.

[15] A.D. Le Claire in: "The permeation of gases through solids. I - Principles", AERE-R 9911 Harwell, Oxfordshire (1981).

[16] F. Waelbroeck in: "Ïnfluence of bulk and surface phenomena on the hydrogen permeation through metals", KFA Jülich report Jül-1966.

[17] E. Serra, A. Perujo, J. Nucl. Mater. 223 (1995) 157.

[18] E. Serra, A. Perujo, J. Nucl. Mater. 240 (1997) 215.

[19] E. Serra, A. Perujo and K. S. Forcey, Vuoto 3 (1997) 18.

[20] M. Caorlin in: "Hydrogen interaction with TiC-coated metals for fusion technology application". Ph.D. Thesis, 1992.

[21] P.M. Richards, S.M. Myers, W.R. Wampler, D.M. Follstaedt, J. Appl. Phys. 65 (1989) 180

[22] L.A. Sedano, K. Douglas, A. Perujo and G.A. Esteban in: "Modelling of the deuterium transient release after plasma implantation shots in the martensitic steel DIN 1.4914 (MANET). Submitted for publication in J. Nucl. Mater.

[23] D.M. Grant, D.L. Cummings and D.A. Blackburn, J. Nucl. Mater. 152 (1988) 139.

[24] E. Rota, F. Waelbroeck, P. Wienhold and J. Winter, J. Nucl. Mater. 111 & 112 (1982) 233.

[25] M. Braun, B. Emmoth, F. Waelbroeck and P. Wienhold, J. Nucl. Mater. 93 & 94 (1980) 861.

The mission of the JRC is to provide customer-driven scientific and technical support for the conception, development, implementation and monitoring of EU policies. As a service of the European Commission, the JRC functions as a reference centre of science and technology for the Union. Close to the policy-making process, it serves the common interest of the Member States, while being independent of special interests, whether private or national.

EUROPEAN COMMISSION
JOINT RESEARCH CENTRE